Variability of the Observed Midlatitude Storm Tracks in Relation to Low-Frequency Changes in the Circulation Pattern

NGAR-CHEUNG LAU

Geophysical Fluid Dynamics Laboratory/NOAA, Princeton University, Princeton, New Jersey

(Manuscript received 29 October 1987, in final form 28 March 1988)

ABSTRACT

The principal modes of month-to-month variability of the wintertime storm tracks over the North Pacific and North Atlantic are identified by empirical orthogonal function analysis of the root-mean-square statistics of bandpass (2.5–6 day) filtered geopotential height data for 19 yr. One of the two leading modes depicts fluctuations in the level of synoptic-scale activity without any noticeable spatial displacement of the storm track axes, whereas the other mode is associated with meridional shifts of the storm tracks from their time-averaged positions. Higher order modes are indicative of diversion or truncation of cyclone tracks in particular geographical regions.

It is demonstrated that the leading storm track modes are linked to some of the best-known monthly averaged teleconnection patterns. The dipolar western Pacific and western Atlantic patterns for the monthly mean flow are seen to be accompanied by marked changes in the intensity of the storm tracks over the western oceans, whereas the more wave-like Pacific/North American and eastern Atlantic teleconnection patterns are coincident with north–south displacements of the storm track axes over the eastern oceans. The representative synoptic scenarios for various storm track modes are portrayed using composite charts. These patterns illustrate the strong modulation of the trajectory of weather systems by the intensity and steering action of the monthly averaged flow field, so that the storm tracks are preferentially located at and slightly downstream of the quasi-stationary troughs.

The shape and propagation of the synoptic scale eddies along the changing storm tracks, as well as the barotropic interactions between these disturbances and the monthly mean flow, are diagnosed using composite patterns of extended Eliassen–Palm vectors and eddy-induced geopotential tendencies at 300 mb. It is seen that the synoptic-scale fluctuations are typically crescent-shaped, and sometimes undergo noticeable deformation when they encounter quasi-stationary ridges. In the upper troposphere, enhanced eddy activity is accompanied locally by eastward acceleration, as well as by positive geopotential tendency immediately to the south, and negative geopotential tendency to the north, and vice versa. The distributions of eddy-induced geopotential tendency for individual storm track modes indicate a near inphase relationship between the synoptic scale barotropic forcing and the quasi-stationary flow pattern at 300 mb. The characteristic time scale for this forcing is approximately 7–10 days.

The characteristic circulations at sea level associated with various storm track modes are examined using composite charts of the sea level pressure field. Some of these composites resemble the patterns associated with the North Pacific and North Atlantic Oscillations.

1. Introduction

The wintertime climatology of transient fluctuations on subweekly time scales and their relationship with the midlatitude tropospheric stationary waves have been documented in a series of observational studies by Blackmon et al. (1977, 1984a, 1984b) and Lau (1978). By mapping the root-mean-square (rms) and covariance statistics as well as one-point teleconnection patterns based on time-filtered data which retain periods within the 2.5–6 day band, these authors reported that the most active disturbances tend to travel eastward through continuous phase propagation within two elongated zones spanning the North Pacific and North Atlantic (see stippled regions in Fig. 1). These maritime sites are characterized by maximum temporal variability in geopotential height, meridional wind, temperature and vertical motion on synoptic time scales. The most vigorous transports of heat and vorticity by high-frequency eddies also take place in these regions. It was further noted that the centers of enhanced eddy activity depicted in Fig. 1 coincide closely with the principal midtropospheric "storm tracks," as inferred independently from earlier surveys of the trajectories of individual cyclone centers (e.g., Petterssen 1956). Hence, the geographical distributions of the temporal variance and covariance fields for a certain time period are good descriptors of the location and intensity of the storm tracks during that period. More recently, Wallace et al. (1988) have pointed out that, since the propagation of both cyclones and anticyclones con-

Corresponding author address: Dr. Ngar-Cheung Lau, Geophysical Fluid Dynamics Laboratory, Princeton University, P.O. Box 308, Princeton, N.J. 08542.

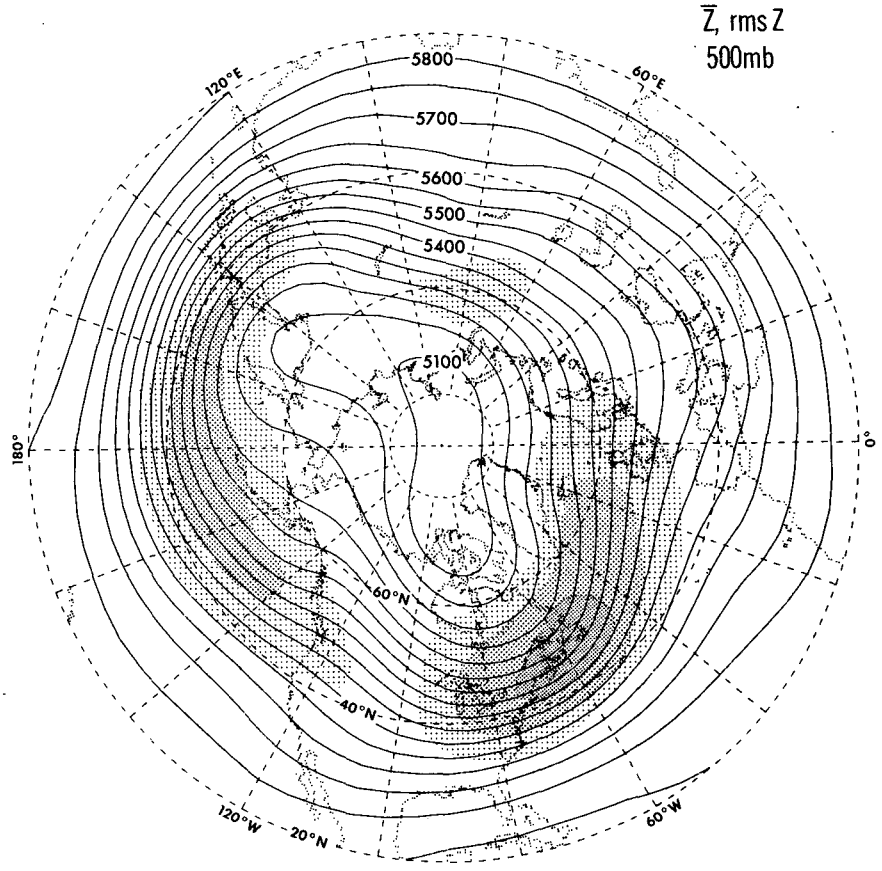

FIG. 1. Climatological distributions of the wintertime 500 mb height (contours) and rms of bandpass filtered 500 mb height (stippling). Contour interval for the time averaged height field is 50 m. The rms values falling within the ranges of 50–60, 60–70 and >70 m are indicated by light, medium and dense stippling, respectively.

tributes to the temporal second-moment statistics, the maxima in such statistics should more properly be referred to as "baroclinic waveguides," which make no explicit inference on the polarity of the fluctuations concerned. However, these authors demonstrated that the propagation characteristics of positive and negative geopotential height anomalies through these baroclinic waveguides are very similar. Hence, in conformity with the terminology adopted in a majority of the published works on this subject, we shall continue to refer to the elongated maxima in the rms of bandpass (2.5–6 day) filtered geopotential height as the "storm tracks," with the understanding that these storm tracks portray preferred migration paths of both positive and negative synoptic-scale perturbations.

The climatological positions of the storm tracks are intimately related to the configuration of the time-mean flow, as represented in Fig. 1 by the time averaged 500 mb geopotential height contours. It is seen that the Pacific and Atlantic storm tracks initiate in the vicinity of the stationary troughs over eastern Asia and eastern North America, and terminate near the stationary ridges over the west coasts of North America and Europe, respectively. The principal storm tracks hence lie downstream and slightly poleward of the vertical and horizontal shear zones associated with the quasi-permanent jet streams over Japan and the eastern United States seaboard. Modeling studies by Simmons and Hoskins (1978), among others, suggest that the structure and transport characteristics of transient eddies along the storm tracks may be interpreted in terms of the life cycles of eastward propagating baroclinic waves. The strong geographical dependence of these baroclinic modes on the longitudinal phase of the stationary wave is demonstrated by Fredericksen (1979), who performed a series of instability analyses using zonally asymmetric basic states.

The discussion above pertains to the long-term averaged behavior of the storm tracks and the stationary flow. Inspection of the counterparts of Fig. 1 for individual seasons or synoptic situations reveals considerable variability from the climatological scenario. For instance, Blackmon et al. (1977, Figs. 12 and 13) pointed out that the Atlantic and Pacific storm tracks

were located south of their time-mean positions during the 1965/66 and 1969/70 winter seasons, respectively. Such displacements in the storm track axes occurred in conjunction with similar shifts in the seasonally averaged jet streams. Furthermore, the analysis by Wallace and Gutzler (1981, Table 3) indicates that the seasonally averaged flows for the 1965/66 and 1969/70 winters resemble the Eastern Atlantic (EA) and Pacific/North American (PNA) teleconnection patterns, respectively. These teleconnection patterns correspond to two of the most prevalent modes of wintertime geopotential height variability on monthly and seasonal time scales, and are each associated with a well-defined set of geographically fixed nodes and antinodes. Hence, there exists some rudimentary evidence linking the slowly varying component of the circulation with systematic changes in the orientation and/or intensity of the storm tracks. This notion is substantiated by synoptic case studies of blocking ridges by Green (1977), Illari (1984), Dole (1986), Mullen (1987), and Holopainen and Fortelius (1987), among others. These investigations provided ample evidence of the strong modulation of the synoptic-scale disturbances during selected blocking situations. Since most of these studies use rather stringent selection criteria to identify blocking events, the numbers of cases treated therein are necessarily rather limited. Moreover, these blocking phenomena only account for a fraction of the low-frequency variability. Further data diagnoses are therefore needed to provide a full description of the relationships between the low- and high-frequency components of the extratropical circulation.

Observational studies of low-frequency atmospheric variability have mostly been concerned with *first*-moment quantities such as geopotential height, temperature or wind. In view of the considerable variability of the storm tracks described above, and noting the rich amount of information on storm track behavior extractable from variance and covariance statistics, it would be of interest to explore the variability of *second*-moment statistics as well. Since stable estimates of these higher statistical moments often require long data records, previous attempts to document the interannual changes of rms and eddy flux statistics were somewhat hindered by the limited sample size then available. Furthermore, it was difficult to interpret the variability of higher-moment quantities in the absence of a conceptual framework founded on synoptical and dynamical principles. As more extended observational datasets become accessible, and with the advent of novel diagnostic tools designed for delineating various facets of local eddy-mean flow interactions, this is an opportune time for undertaking a more systematic analysis of the dominant modes of variability of the storm tracks, as well as the relationship between such modes and the quasi-stationary circulation. These issues are addressed in the present study by identifying the spatial patterns of the recurrent month-to-month changes in time-filtered rms statistics, and by associating these patterns with some of the well-known teleconnection patterns for the monthly averaged circulation, such as those described in Wallace and Gutzler (1981), Esbensen (1984), and Barnston and Livezey (1987). Dynamical interactions between the monthly mean circulation anomalies and transient disturbances with subweekly time scales will be examined using local Eliassen–Palm vectors and eddy-induced geopotential height tendencies.

2. Datasets

The primary database for this study consists of twice-daily grid point analyses produced by the U.S. National Meteorological Center. The variables selected include geopotential height at 500 and 300 mb, and sea level pressure. The data domain extends from 20°N to the North Pole. The period of coverage extends from January 1963 to December 1981 for 500 mb height and sea level pressure, and from January 1964 to December 1981 for 300 mb height. Temporal data gaps were filled using linear interpolation in time. The winter season is taken to be the 5-month period from November to March. Hence, there are, altogether, 95 individual winter months in the dataset for 500 mb height and sea level pressure, and 90 months in the set for 300 mb height.

In order to accentuate the synoptic scale disturbances with characteristic periods of several days, the medium-pass filter described in Blackmon (1976, Fig. 2 and Table 1) has been applied to the twice-daily time series of the geopotential height and sea level pressure fields. This filter, often referred to in later works as the "bandpass" filter, retains fluctuations with 2.5–6 day periods. The filtered time series for 500 mb height were then partitioned into individual monthly segments, one for every winter month. For each monthly segment, the mean values of that segment were subtracted from all twice-daily data in the same month,[1] and the temporal rms values were then computed for that segment. Hence, one obtains, altogether, 95 data fields, with each field corresponding to the bandpass filtered rms pattern of 500 mb height for a certain winter month.

Throughout this study, removal of the climatological seasonal cycle from the monthly mean or rms fields has been accomplished by subtracting the long-term averaged values for a given calendar month from corresponding values of the same month in individual years.

[1] The monthly means of the bandpass filtered data for each segment are typically several orders of magnitude smaller than the corresponding twice-daily values. These averages were removed from the time series in individual segments simply for the sake of numerical precision.

In summary, we shall be dealing with two types of data fields in this study. The first type consists of monthly mean patterns obtained from averages of unfiltered data. These first-moment statistics describe the slowly evolving component of the circulation. For the sake of brevity, these patterns will be referred as the "monthly mean" fields. The second type is composed of the rms statistics of bandpass filtered data. Such second-moment statistics depict the spatial configuration of the storm tracks in individual months, and will be collectively labeled as the "rms" fields in the following discussion.

3. Principal modes of variability of the storm tracks and their relationship with the monthly averaged circulation

a. Eigenvectors of the rms fields

Characteristics of the most recurrent changes in the location and intensity of the oceanic storm tracks are identified here using empirical orthogonal functions (EOFs), which yield a set of spatial patterns (i.e., the eigenvectors) and temporal coefficients accounting for a substantial fraction of the variance of the dataset under investigation. Readers unfamiliar with this analysis technique are referred to a concise summary of the basic methodology given in Kutzbach (1967). For the present application, the analysis was performed on the temporal covariance matrix computed using the rms fields of bandpass filtered 500 mb height for 95 individual winter months (see section 2 for details). In view of the organization of the enhanced bandpass eddy activity into two distinct storm tracks, one over the North Pacific and the other over the North Atlantic (see Fig. 1), the EOF analysis was executed separately for the Pacific and Atlantic sectors. Each of these maritime sectors has a longitudinal span of 150°, and a latitudinal span of 50° (from 20° to 70°N). The Pacific sector extends from 100°E to 110°W, whereas the Atlantic sector extends from 110°W to 40°E. The spatial variations in each domain of analysis are depicted at 126 grid points, which are chosen such that they represent approximately equal areas. These grid points lie on latitude rows spaced at 5° intervals. The longitudinal positions of the points along neighboring latitude rows are staggered. The grid resolution along the zonal direction is 10° longitude between 20° and 40°N, and 20° longitude between 45° and 70°N. The climatological seasonal cycle has been removed from the rms fields prior to the EOF analysis.

Figures 2 and 3 show the spatial distributions of the four leading eigenvectors for the Pacific and Atlantic sectors, respectively. We shall hereafter refer to the first four EOF modes for the Pacific Basin as P1, P2, P3 and P4. Similarly, the corresponding modes in the Atlantic sector are labeled as A1, A2, A3 and A4. The percentage of variance explained by the individual modes is given at the top of each panel. It is seen that

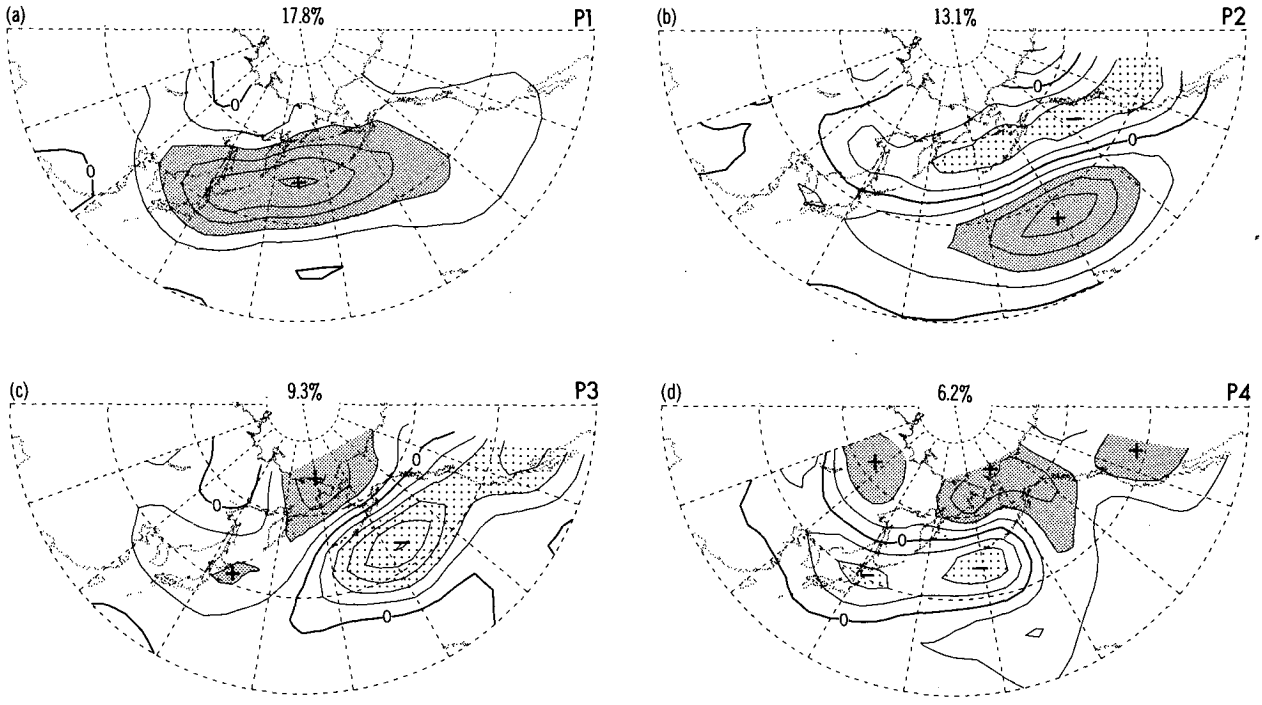

FIG. 2. Distributions of the four leading eigenvectors of the rms of bandpass filtered 500 mb height for the Pacific Basin. Extrema are highlighted by dense or light stippling. The percentage of variance explained by each eigenvector is indicated at the top of the corresponding panel. Arbitrary units.

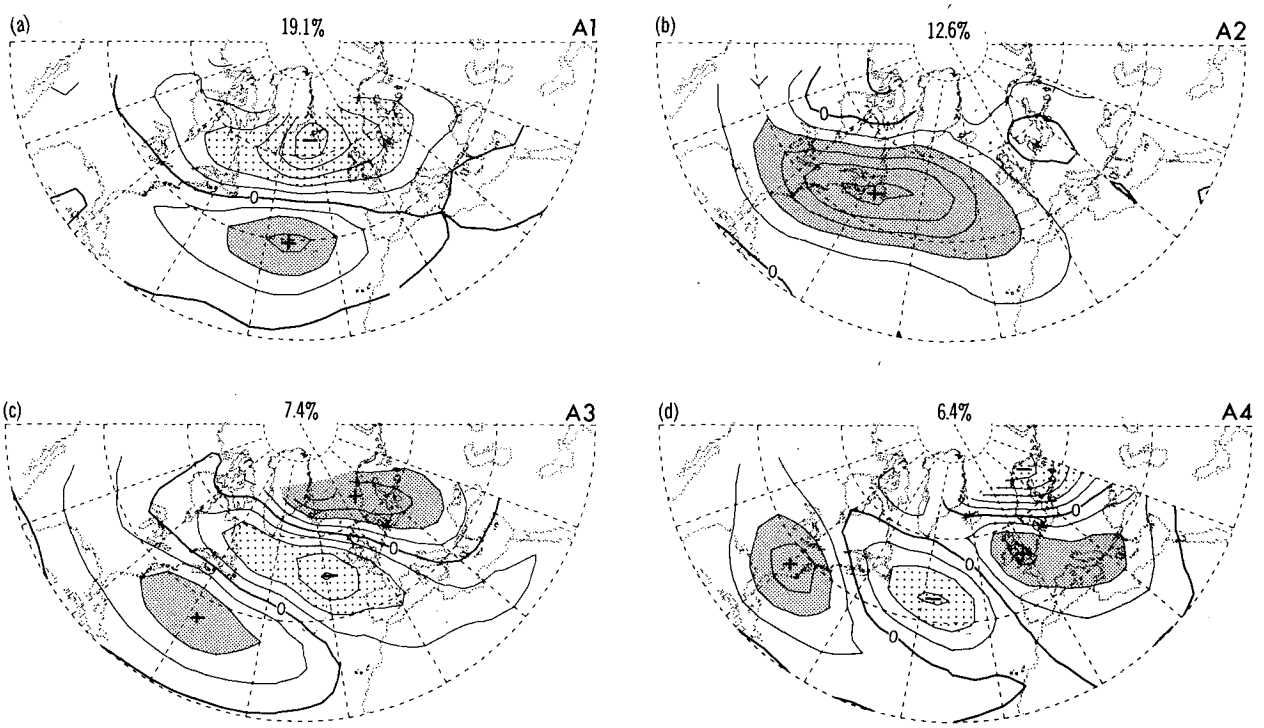

FIG. 3. As in Fig. 2, but for eigenvectors of the Atlantic Basin.

the first four eigenvectors collectively account for approximately 46% of the total variance in each domain.

Inspection of the panels in Figs. 2 and 3 reveals the following types of spatial variability for the storm tracks:

- P1 and A2: These eigenvectors are characterized by a monopole pattern. The locations of the elongated extrema in these modes correspond closely with the climatological positions of the major storm track axes (see Fig. 1). These eigenvectors portray the strengthening or weakening of eddy activity, with almost no spatial displacement of the storm track axes from their long-term averaged positions.
- P2 and A1: These patterns are noted for the presence of a dipole structure over the central and eastern parts of the ocean basins. The pair of extrema in each pattern tend to straddle the climatological storm track axis. These eigenvectors depict northward or southward migration of the storm tracks from their time-mean positions.
- P3: This eigenvector pattern consists of an extremum situated over the eastern edge of the Asian land mass with a southwest-to-northeast orientation, and a second elongated extremum of the opposite polarity extending from the dateline to the western United States. In its positive phase, this mode is associated with deflection of the Pacific storm track towards the Bering Sea/Alaskan region, and weakened eddy activity over the eastern Pacific.
- A3 and A4: These modes are composed of multiple centers of action with alternating polarities. They are suggestive of wave-like modulation of eddy activity, with above and below normal eddy amplitudes occurring at preferred sites.

b. Relating the storm track eigenvectors to the monthly mean flow

The month-to-month variation of each spatial mode displayed in Figs. 2 and 3 during the 1963–81 period may be represented by a time series of 95 temporal coefficients. For a certain winter month m in the 95-month dataset, the temporal coefficient associated with a certain mode e is given by the spatial covariance between the eigenvector for e and the anomalous rms pattern during month m. The storm track behavior in those months with high positive coefficients for mode e would exhibit many of the modal characteristics associated with e. Conversely, large negative coefficients signify spatial resemblance to the same eigenvector but with the polarities of the extrema reversed. In order to discern the relationships between the monthly averaged circulation and the individual EOFs shown above, temporal correlation coefficients have been computed between the 95 time-coefficients for each eigenvector and the concurrent 95 monthly averaged 500 mb height values at each grid point of the data domain. The climatological seasonal cycle has been removed from the monthly mean values prior to these calculations. The geographical distributions of the correlation values thus

obtained are mapped in Figs. 4 and 5 for the Pacific and Atlantic eigenvectors, respectively. For a given eigenvector, a positive region in the corresponding panel indicates that this mode tends to occur in conjunction with above normal monthly mean heights in that region. Analogously, negative regions in these correlation patterns imply an association of below normal heights with the eigenvector in question. To provide a crude measure of the statistical significance of the correlation coefficients displayed in Figs. 4 and 5, we make the conservative assumption that there are only two degrees of freedom in each 5 month winter, so that the dataset yields a total of 38 degrees of freedom; the corresponding threshold correlation values at the 95% and 99% confidence levels would then be 0.32 and 0.41, respectively.

By comparing the eigenvectors in Figs. 2 and 3 with the corresponding correlation maps in Figs. 4 and 5, we note the following sets of relationships between the storm tracks and the monthly mean flow:

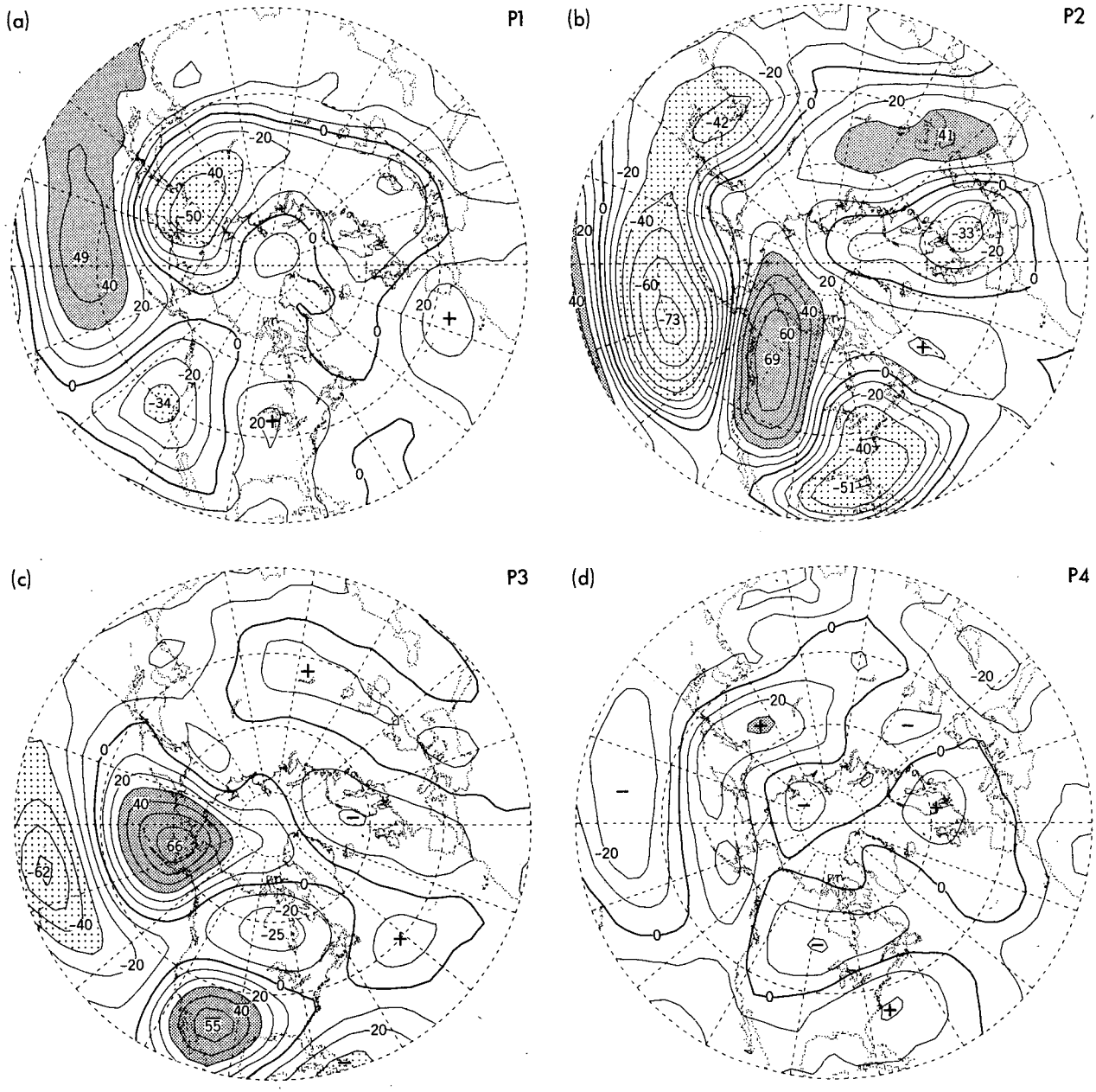

FIG. 4. Distributions of the correlation coefficients (in percent) between the temporal coefficients of the four leading Pacific storm track eigenvectors and the monthly averaged 500 mb height values at individual grid points. Contour interval: 10%. Regions with correlation values above +30% and below −30% are highlighted by dense and light stippling, respectively.

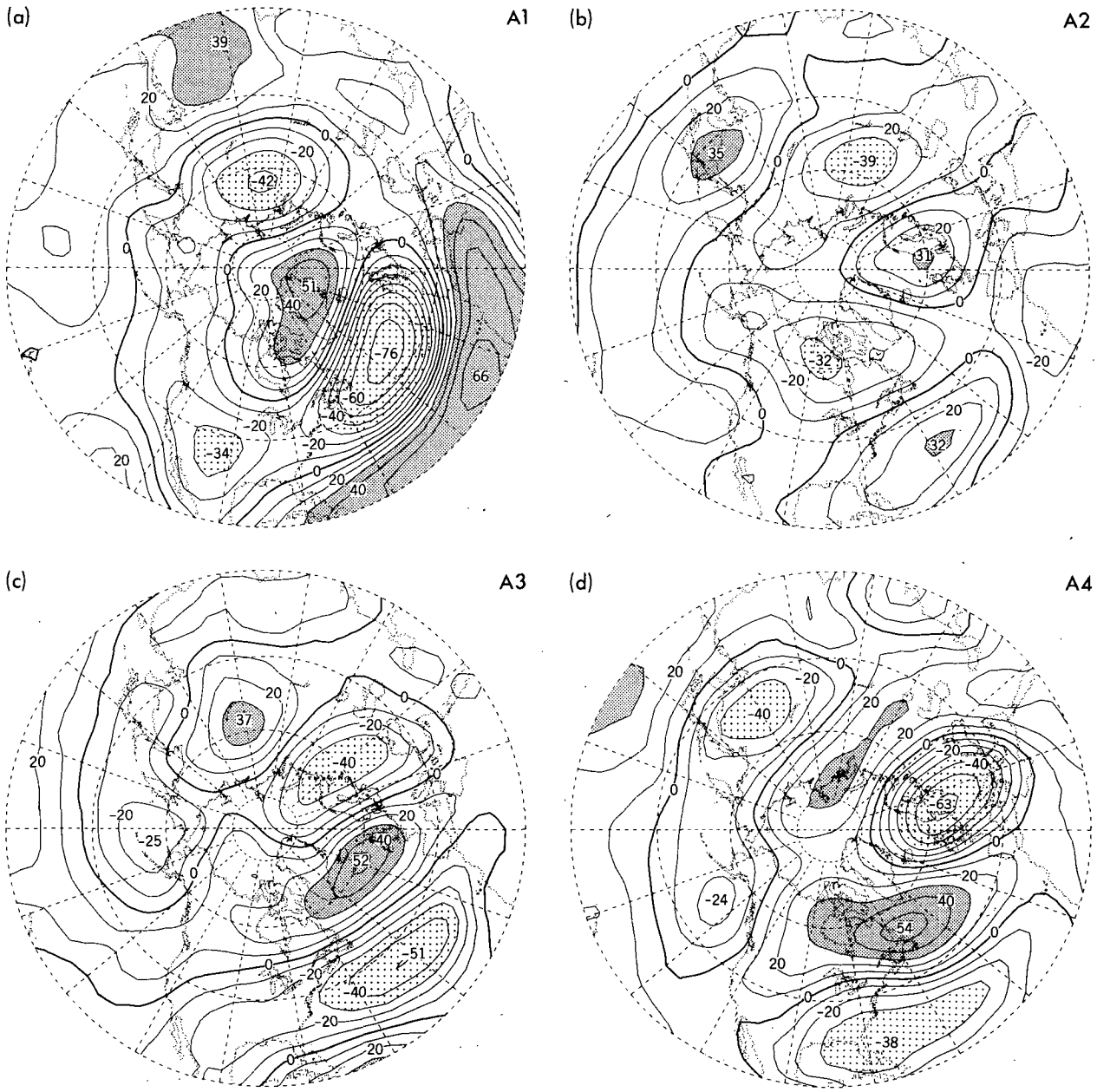

FIG. 5. As in Fig. 4, but for the four leading Atlantic storm track eigenvectors.

- P1 and A2: These eigenvectors are seen to be associated with dipolar structures in the monthly mean circulation anomaly over the western portion of the Pacific and Atlantic Basins (Figs. 4a and 5b). These dipoles are oriented along a predominately north–south axis, and tend to straddle the elongated extrema appearing in the corresponding eigenvectors for the rms statistics (Figs. 2a and 3b). The intensity of eddy activity is hence positively correlated with the strength of the monthly mean westerly flow along the storm track. For the Pacific sector (Fig. 4a), the two opposite poles lie in the proximity of the centers of action associated with the western Pacific (WP) pattern (Wallace and Gutzler 1981, hereafter referred to as WG, Fig. 24). The comparatively weaker correlation pattern associated with A2 (Fig. 5b) exhibits some spatial resemblance to the teleconnection chart for the western Atlantic (WA) pattern, as documented by WG (Fig. 20).
- P2 and A1: Among the various correlation charts displayed in Figs. 4 and 5, the patterns associated with these eigenvectors contain some of the strongest correlation coefficients. It is seen that southward migration of the storm track axes is accompanied by

negative monthly mean height departures in the midlatitude (40°–50°N) oceans, with strengthened monthly mean westerlies along approximately 30°N, and weakened westerlies within the zone between 50° and 60°N. Conversely, northward movement of the storm tracks occurs in conjunction with above normal monthly mean heights in the middle latitudes, and with northward shifts in the westerly jet stream. The characteristic monthly mean flow associated with P2 (Fig. 4b) bears a striking resemblance to the Pacific/North American (PNA) teleconnection pattern (WG, Fig. 16). The maritime centers of action in the monthly mean circulation corresponding to the A1 mode (Fig. 5a) coincide with those appearing in the eastern Atlantic (EA) pattern (WG, Fig. 12)

- P3: The positive phase of this eigenvector is associated with above normal monthly mean heights over the Bering Sea region and the United States–Mexican border, below normal heights over the subtropical central Pacific, and reduced midlatitude westerly flow in the central and eastern Pacific (Fig. 4c). The principal features in Fig. 4c are similar to those appearing in the Pacific (P) pattern at the 500 mb level, as described by Hsu and Wallace (1985; left panel of their Figs. 2 and 8). These authors noted that this characteristic pattern may be linked to the preferred occurrence of blocking ridges over the Aleutians.
- A3 and A4: The wave-like configuration of the extrema in the eigenvector patterns (Figs. 3c and 3d) bear an apparent quadrature spatial relationship with the corresponding monthly mean geopotential height anomalies (Figs. 5c and 5d), with regions of enhanced maritime eddy activity being straddled by a positive height anomaly to the south and a negative anomaly to the north, and vice versa. Strengthened (weakened) storm tracks are hence coincident with westerly (easterly) anomalies in the monthly mean zonal flow. The characteristic monthly mean circulation associated with A4 (Fig. 5d) resembles the WA teleconnection pattern (WG, Fig. 20).

In summary, the results presented in Figs. 2–5 demonstrate that the principal modes of variability of the storm tracks exhibit well-defined relationships with some of the best-known teleconnection patterns constructed using monthly averaged data. An ubiquitous feature in these sets of charts is the collocation of above normal eddy activity and westerly anomaly in the monthly mean circulation. This relationship holds for the WP, WA and P patterns, in which the dipole structure in the height field modulates both the monthly mean zonal wind and the storm track intensity. It also holds for the PNA and EA patterns, in which the anomaly centers over the midlatitude Pacific and Atlantic are accompanied by meridional shifts in both the jet stream and storm track axes, as well as for the wave-like patterns associated with A3 and A4.

The salient relationships between the storm track eigenvectors and the teleconnection patterns for the monthly averaged flow are further quantified in Table 1, in which is shown the temporal correlation matrix between the time coefficients for individual eigenvectors (see beginning of this subsection) and the five teleconnection pattern indices documented in WG. The teleconnection pattern indices were constructed following exactly the definitions given in WG. Such definitions entail a linear combination of the normalized monthly mean height anomalies at the centers of action for individual patterns, with the relative polarity of the centers being taken into consideration. The pattern indices computed in this manner depict the month-to-month evolution of the strength and polarity of each teleconnection pattern. The climatological seasonal cycle has been removed in all of the above calculations. In order to highlight the stronger correlation values, only those coefficients with absolute values equal to or exceeding 30% are displayed in Table 1. According to the crude estimate made earlier, this criterion corresponds to a significance level of approximately 95%. The eigenvectors P3 and P4 exhibit no significant correlation with any of the five teleconnection patterns and are hence not included in the table. This tabulation confirms the strong connections alluded to earlier between WP and P1, PNA and P2, EA and A1, and WA and A4. Generally speaking, the WP and PNA patterns exhibit well-defined, one-to-one relationships with the Pacific eigenvectors, whereas the EA and WA patterns are each associated with multiple Atlantic eigenvectors. The latter result is partially a consequence of the substantial overlap between the pattern centers for EA and WA (see WG, Fig. 26). It is also worth noting that a few of the eigenvectors (namely, P2, A2 and A4) are, to a lesser degree, also correlated with the Eurasian (EU) pattern. These relationships are to be expected in view of the fact that the EU pattern exhibits non-negligible correlations with each of the four remaining teleconnection indices considered here (see WG, last column of their Table 4).

The possibility of temporal relationships between the storm track eigenvectors for the Pacific Basin and those for the Atlantic Basin has been investigated by cross correlating the temporal coefficients for P1, P2, P3 and P4 with the coefficients for A1, A2, A3 and A4. The resulting matrix (not shown) does not contain any significant correlation value. The storm track eigenvectors for the two ocean basins are hence independent of each other. These calculations provide a posteriori justification for treating the variability of the rms fields in each ocean separately in this study.

c. Composite patterns of monthly mean and rms statistics for 500 mb height

The typical synoptic scenarios for the eigenvectors described above are depicted here using composite

TABLE 1. Correlation coefficients (in percent) between monthly temporal coefficients of leading storm track eigenvectors (P1, P2, A1, A2, A3 and A4) and monthly indices of the western Pacific (WP), Pacific/North American (PNA), eastern Atlantic (EA), western Atlantic (WA) and Eurasian (EU) teleconnection patterns documented in Wallace and Gutzler (1981). Correlations with absolute values below 30% have been omitted from this tabulation.

Teleconnection patterns	Pacific eigenvectors		Atlantic eigenvectors			
	P1	P2	A1	A2	A3	A4
WP	−48					
PNA		+68				
EA			−61		+42	
WA				−30	+30	+50
EU		+41		−39		+32

charts. For the sake of brevity, we shall henceforth focus our attention on the P1, P2 and P3 modes in the Pacific, and the A1, A2 and A4 modes in the Atlantic. These particular eigenvectors are selected mainly on the basis of their close ties with the attendant monthly mean circulation (see Figs. 4, 5 and Table 1). In constructing the composite charts for the positive phase of a given eigenvector mode, the monthly temporal coefficients (see definition in section 3b) for this eigenvector were ranked according to their magnitudes. Those 10 months with the largest *positive* temporal coefficients were then identified, and the meteorological quantity of interest was then averaged over these 10 months to form a composite field, hereafter referred to as the *high* composite. Conversely, the negative phase of the eigenvector is portrayed by averaging over those 10 months with the largest *negative* temporal coefficients, so as to form the *low* composite. The winter months entering into the high and low composites for different eigenvectors are listed in Table 2. The high and low composites of monthly averaged 500 mb geopotential height (contours) and the corresponding filtered rms values (stippling) are shown in Fig. 6 for selected Pacific eigenvectors, and in Fig. 7 for the Atlantic modes.

The most striking distinction between the two composites for the P1 mode (Figs. 6a and 6b) is the relaxation of the monthly mean height gradient over the Bering Sea region in the low composite. The weakened monthly mean circulation in Fig. 6b is accompanied by an equally drastic reduction in eddy activity, so that the rms values everywhere in that panel lie below the threshold for the lowest stippling density (i.e., 50 m).

The monthly mean height field in the high composite for P2 (Fig. 6c) is characterized by a broadened trough over the central Pacific, and an amplified ridge along the western seaboard of North America. The corresponding storm track tends to be aligned with the circulation around the midocean trough, and is apparently truncated upon approaching the upstream side of the pressure ridge over the North American coast. The low composite (Fig. 6d) is noted for the zonality of the monthly mean circulation over the eastern Pacific and western Canada. Associated with this flow pattern is the tracking of the transient disturbances along the Aleutians towards the Gulf of Alaska. The storm track in the low composite lies considerably north of its counterpart in the high composite, and penetrates farther east towards the North American coast.

The most prominent feature in high composite for P3 (Fig. 6e) is the pressure ridge extending northward from the Aleutians to the Arctic. Immediately to the south of this anticyclonic regime is a strong trough over the subtropical Pacific. The shape of the storm track in the high composite suggests that the eastward migration of the midlatitude disturbances is impeded near the dateline, with some of them being steered northward along the western flank of the ridge (see

TABLE 2. Lists of winter months with the ten most positive and most negative temporal coefficients for selected storm track eigenvectors. These ten-month groups are used to construct high and low composites of various circulation statistics, respectively. Each winter month in this list is identified by the last two digits of the year, followed by a slash and then by a one- or two-digit number representing the calendar month (1 for January, 2 for February, . . . , 12 for December). The winter months are arranged in descending order of the absolute values for the EOF temporal coefficients.

Pacific eigenvectors						Atlantic eigenvectors					
P1		P2		P3		A1		A2		A4	
High	Low	High	Low	High	Low	High	Low	High	Low	High	Low
71/12	64/12	70/2	77/3	66/11	64/1	68/11	66/11	71/3	78/2	71/11	74/1
70/2	63/2	69/12	75/1	67/3	64/3	66/2	63/1	73/1	67/1	70/2	75/2
66/2	63/1	63/2	64/2	72/2	73/3	81/3	73/2	76/12	68/2	68/1	64/1
65/12	69/1	68/2	71/12	63/1	73/1	70/1	81/1	64/1	63/2	71/3	74/3
68/1	75/1	76/11	63/3	68/1	67/12	65/12	75/12	80/11	69/2	69/2	78/11
70/11	78/2	65/3	68/12	63/12	66/1	77/2	67/11	68/3	81/12	66/1	71/12
76/1	74/12	80/12	75/2	81/12	72/11	64/3	70/3	77/12	69/3	69/11	63/2
66/1	68/11	68/3	76/2	64/12	63/11	66/1	80/12	74/2	77/3	67/12	72/12
65/11	72/3	81/1	76/3	80/12	64/2	68/12	77/11	80/3	65/3	66/12	70/12
69/2	77/11	66/12	71/11	73/11	74/2	78/2	68/3	72/2	69/1	69/12	65/3

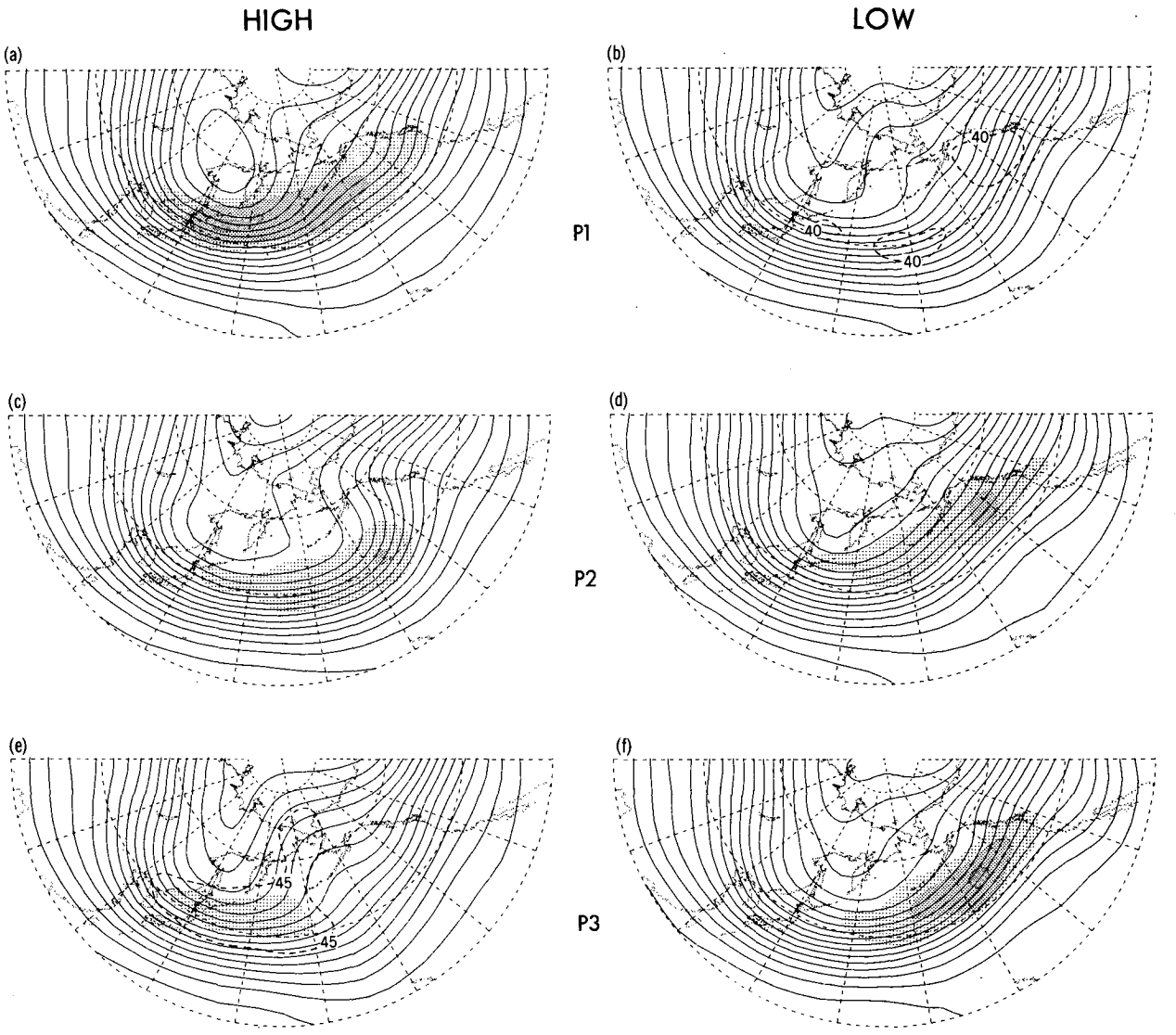

FIG. 6. High composite (left panels) and low composite (right panels) patterns of the monthly mean 500 mb height (contours) and rms of bandpass filtered 500 mb height (stippling) for the Pacific storm track eigenvectors P1, P2 and P3. See section 3c for details of the composite procedure. Contour interval for the 500 mb height field is 50 m. The rms values falling within the ranges of 50–60, 60–70 and >70 m are indicated by light, medium and dense stippling, respectively. Dashed contours in panels (b) and (e) indicate weaker rms values of 40 and 45 m, respectively.

dashed contour in Fig. 6e). A similar orientation of the storm track has been noted by Dole (1986, Fig. 4a) in episodes of persistent positive height anomalies over the North Pacific. The absence of the midocean ridge in the low composite (Fig. 6f) is seen to correspond with frequent passage of active synoptic-scale systems across the eastern Pacific.

In the low composite for A1 (Fig. 7b), the amplified pressure ridge over the eastern Atlantic is seen to be accompanied by a storm track with a southwest–northeast orientation, with much of the eddy activity being confined upstream and poleward of the ridge. Dole (1986, Fig. 5) and Mullen (1987, Fig. 3) have observed a similar relationship between the storm track and the quasi-stationary circulation during typical North Atlantic blocking events. The high composite for A1 (Fig. 7a) is characterized by a broad Atlantic trough and a more zonally oriented storm track. Comparison between the two composites reveals a meridional displacement in the storm track axis by as much as 20° of latitude over the eastern Atlantic.

The monthly mean circulation in the high composite for A2 (Fig. 7c) is distinguished from that in the low composite (Fig. 7d) by the considerable tightening of the height gradients in the former pattern over the Labrador Peninsula and the maritime region off the

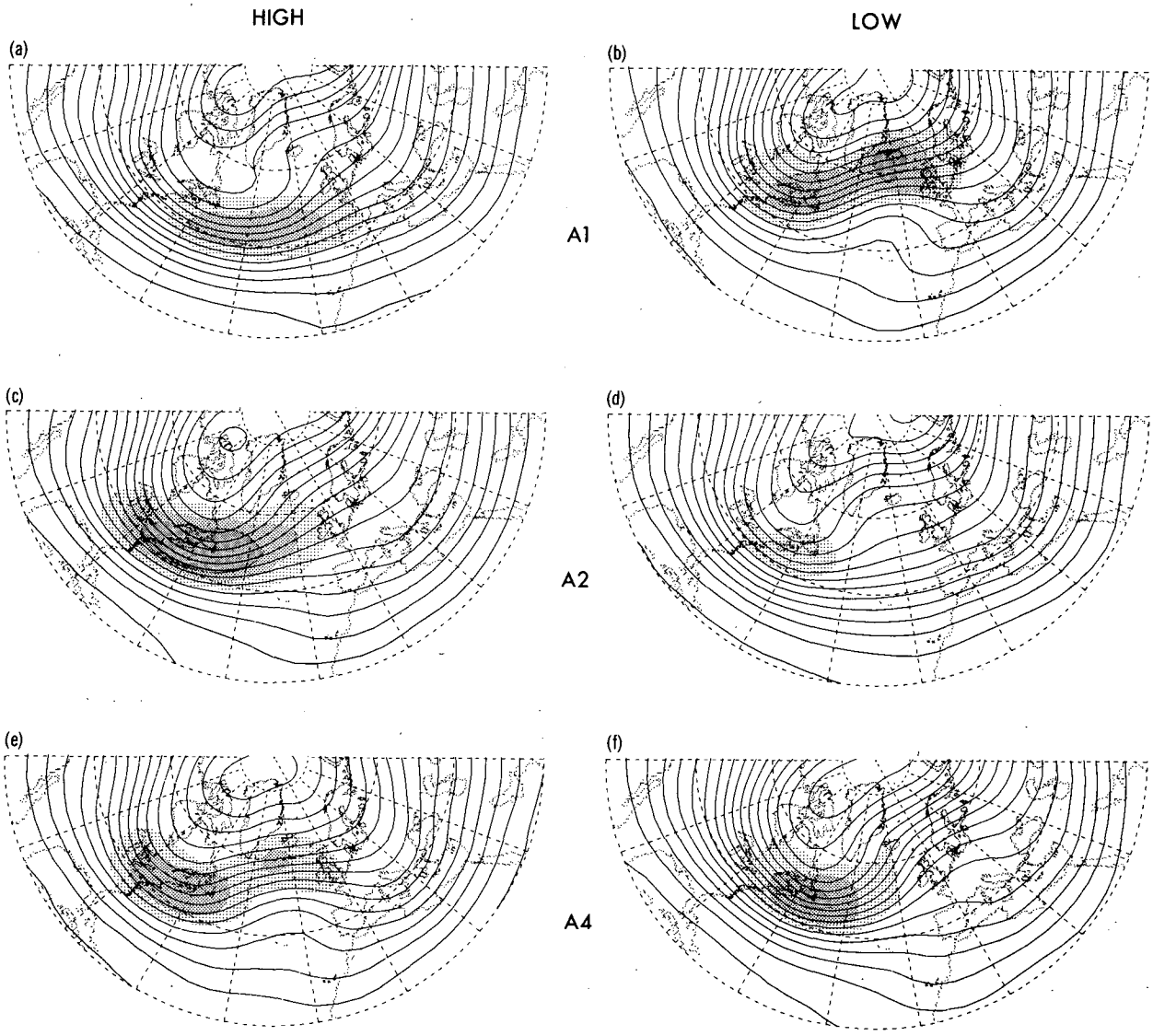

FIG. 7. As in Fig. 6, but for the Atlantic storm track eigenvectors A1, A2 and A4.

southeastern coast of Greenland. Associated with the more intense circulation over eastern Canada in the high composite is a region of vigorous eddy activity, with rms amplitudes reaching as high as 90 m. The level of transient activity in the low composite is much weaker, with rms amplitudes peaking at only about 55 m. The eastward passage of weather disturbances in the low composite appears to be interrupted by the anticyclonic flow pattern occurring over southeastern Greenland.

Comparison of the monthly mean circulation accompanying A4 (Figs. 7e and 7f) suggests a systematic eastward displacement of the long-wave trough and ridge axes in the low composite relative to the corresponding features in the high composite. The other notable distinction between Figs. 7e and 7f is the much stronger jet stream over eastern North America in the low composite. These circulation changes occur in conjunction with the eastward displacement as well as amplitude enhancement of the main center of eddy activity over the eastern seaboard of North America in the low composite.

The underlying theme throughout the above discussion is the strong spatial relationship between the monthly mean flow pattern and the storm tracks. Almost without exception, the synoptic-scale eddies attain maximum amplitudes along a belt of strong prevalent westerlies located slightly downstream of the monthly mean troughs. There is ample evidence in these composite charts (e.g., see Figs. 6c, 6e, 7b and 7d) of the tendency for amplified quasi-stationary ridges to block the advance of weather systems. The marked influence

of the mean flow curvature on the shape of the storm track (e.g., see Figs. 6e, 7b, 7e and 7f) is indicative of the steering effect of the slowly varying circulation on the transient waves.

d. The Eurasian sector

The pattern in Fig. 1 indicates a third region of enhanced synoptic scale activity in Siberia. In order to offer a more complete survey of the variability of wintertime storm tracks in the Northern Hemisphere, and to test whether the relationships between the oceanic storm tracks and the monthly mean flow are applicable to the Eurasian sector, we show in Fig. 8 the distributions of (a) the first eigenvector for the rms of bandpass filtered 500 mb height over Eurasia, and (b) the correlation coefficients between the temporal coefficients for the first eigenvector and the monthly mean 500 mb heights at individual grid points. The procedures for the eigenvector analysis are identical to those outlined in section 3a, with the exception that the domain is now taken to be the region situated between the Greenwich Meridian and 150°E. In analogy to P1 (Fig. 2a) and A2 (Fig. 3b), the leading eigenvector for the Eurasian region, which accounts for 15.1% of the domain-integrated variance, is characterized by a monopole pattern. The primary center of extremum in Fig. 8a is located near the climatological position of

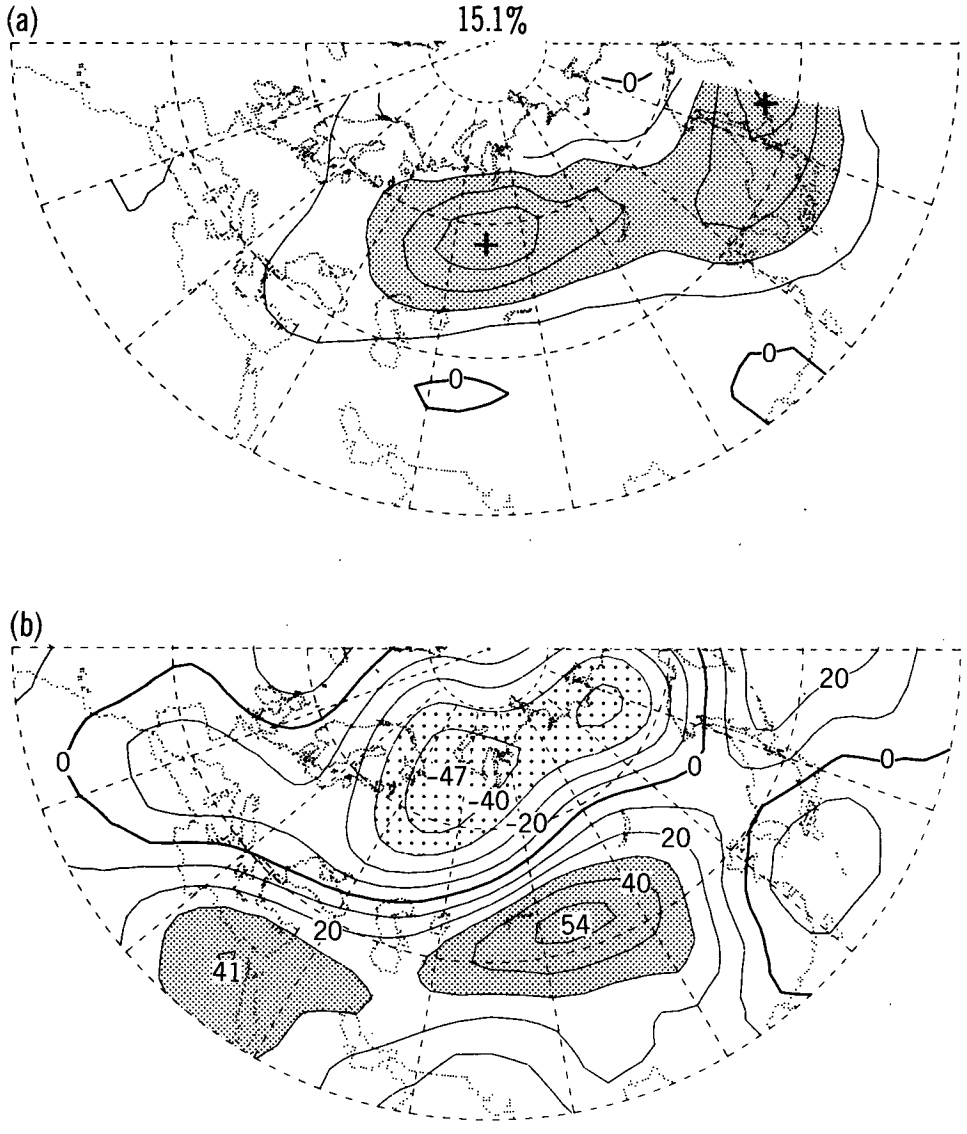

FIG. 8. Distributions of (a) the leading eigenvector of the rms of bandpass filtered 500 mb height for the Eurasian sector, arbitrary units; and (b) correlation coefficients (in percent) between the temporal coefficients for the leading eigenvector and the monthly averaged 500 mb height values at individual grid points; contour interval is 10%.

the Siberian storm track (see Fig. 1). This distribution suggests that the principal mode of variability in this region is associated with enhancement or reduction in the intensity of the storm track, but with little spatial displacement from its time mean location. The characteristic monthly mean circulation accompanying this eigenvector mode is portrayed in Fig. 8b, which exhibits a dipole-like pattern. The primary extrema in this correlation chart coincide with the centers of action associated with the intermonthly signal of the Northern Asian (NA) teleconnection pattern (Esbensen 1984, Fig. 6a). Comparison between the two panels in Fig. 8 reveals that eddy activity increases when the monthly mean heights over Mongolia are above normal, and the heights over the Arctic coasts of the Soviet Union are below normal, so that strengthened mean westerlies prevail along the storm track. These results confirm that the Eurasian sector exhibits some of the same storm track/mean flow relationships discerned over the two ocean basins.

4. Dynamical interactions between the storm tracks and the monthly mean circulation

We now investigate in some detail the properties of synoptic-scale eddies during the anomalous episodes identified in section 3. Particular emphasis is placed on the implications of anomalous eddy behavior on dynamical interactions between the low- and high-frequency components of the atmospheric circulation. We focus our attention on the circulation at 300 mb, and limit our diagnosis to barotropic processes only. The relevant circulation features at sea level will be documented in section 5, whereas the important problem concerning the role of baroclinic processes in atmospheric variability will not be attempted here.

Various analysis tools aimed at diagnosing eddy behavior and eddy-mean flow interactions have been developed during the recent years. Holopainen (1984, section 4) has offered a comprehensive review of such diagnostic tools. In the present study, we shall make use of the extended Eliassen–Palm vectors to illustrate the characteristics of transient eddies in various types of synoptic scenarios, and then apply the insights thus gained to interpret the eddy-forced geopotential tendencies for the same set of scenarios.

a. Extended Eliassen–Palm vectors

The extended Eliassen–Palm vectors were devised by Hoskins et al. (1983) for illustrating local interactive processes between transient eddies and the time mean flow. Variants of the local Eliassen–Palm vectors, hereafter referred to as **E**, have thereafter been introduced by different investigators (e.g., Plumb 1985, 1986; Henden and Hartmann 1985; Trenberth 1986). In this study, we shall use Trenberth's version of **E**, with the horizontal components being given by $\frac{1}{2}(\overline{v'^2} - \overline{u'^2})\mathbf{i} - \overline{u'v'}\mathbf{j}$. Here u and v are the zonal and meridional wind components, respectively, the overbars represent time averages, and the primes denote deviations from the corresponding time mean quantities. Trenberth (1986) showed that the **E** vector defined in this manner provides useful information on the following eddy properties:

- The eddy-induced accelerations of the zonal and meridional wind components due to barotropic processes are given by the divergence and curl of **E** (i.e., $\nabla \cdot \mathbf{E}$ and $\mathbf{k} \cdot \nabla \times \mathbf{E}$), respectively.
- The major or minor axis of the anisotropic part of the eddy stress tensor, from which the characteristic shape and horizontal tilt of the eddy can be deduced, subtends with the zonal direction an angle equal to one-half of the corresponding angle for the **E** vector (see Hoskins et al. 1983).
- In the barotropic case, the group velocity of the transient disturbances relative to the local time mean flow is parallel to **E**.

The eddy behavior associated with various storm track modes identified in section 3a is examined here using composite charts of the **E** and eddy kinetic energy $[\frac{1}{2}(\overline{u'^2} + \overline{v'^2})]$ fields at 300 mb. The composite procedure is almost identical to that used in constructing the composite patterns of monthly mean and rms heights at 500 mb (see section 3c).[2] For each of the winter months constituting the high and low composites for a given storm track mode, the variance and covariance statistics $\overline{u'^2}$, $\overline{v'^2}$ and $\overline{u'v'}$ were computed. Here the time averaging operation is performed over the given month, and the eddies are defined as departures from the corresponding monthly mean. The twice-daily zonal and meridional wind components were computed from the bandpass filtered geopotential height field at 300 mb using the geostrophic approximation. The wind statistics for individual months were then summed over each of the 10-month groups, and the resulting **E** and eddy kinetic energy patterns are displayed using arrows and stippling, respectively. The composite patterns thus obtained are shown in Figs. 9 and 10 for the Pacific and Atlantic storm track modes, respectively.

Comparison between the stippling patterns in Figs. 6 and 7, and those in Figs. 9 and 10 reveals that the regions of enhanced geopotential height variability are also characterized by high eddy kinetic energy. The strong similarity between the time–space behavior of the rms height and eddy kinetic energy fields implies

[2] Since the 300 mb height data were not available for 1963, those winter months listed in Table 2 which fall within this particular year have been replaced by months in the 1964–81 period with rankings just lower than the months appearing in the last row of this table. The reconstituted 10-month groups for individual storm track eigenvectors were then used to construct composites.

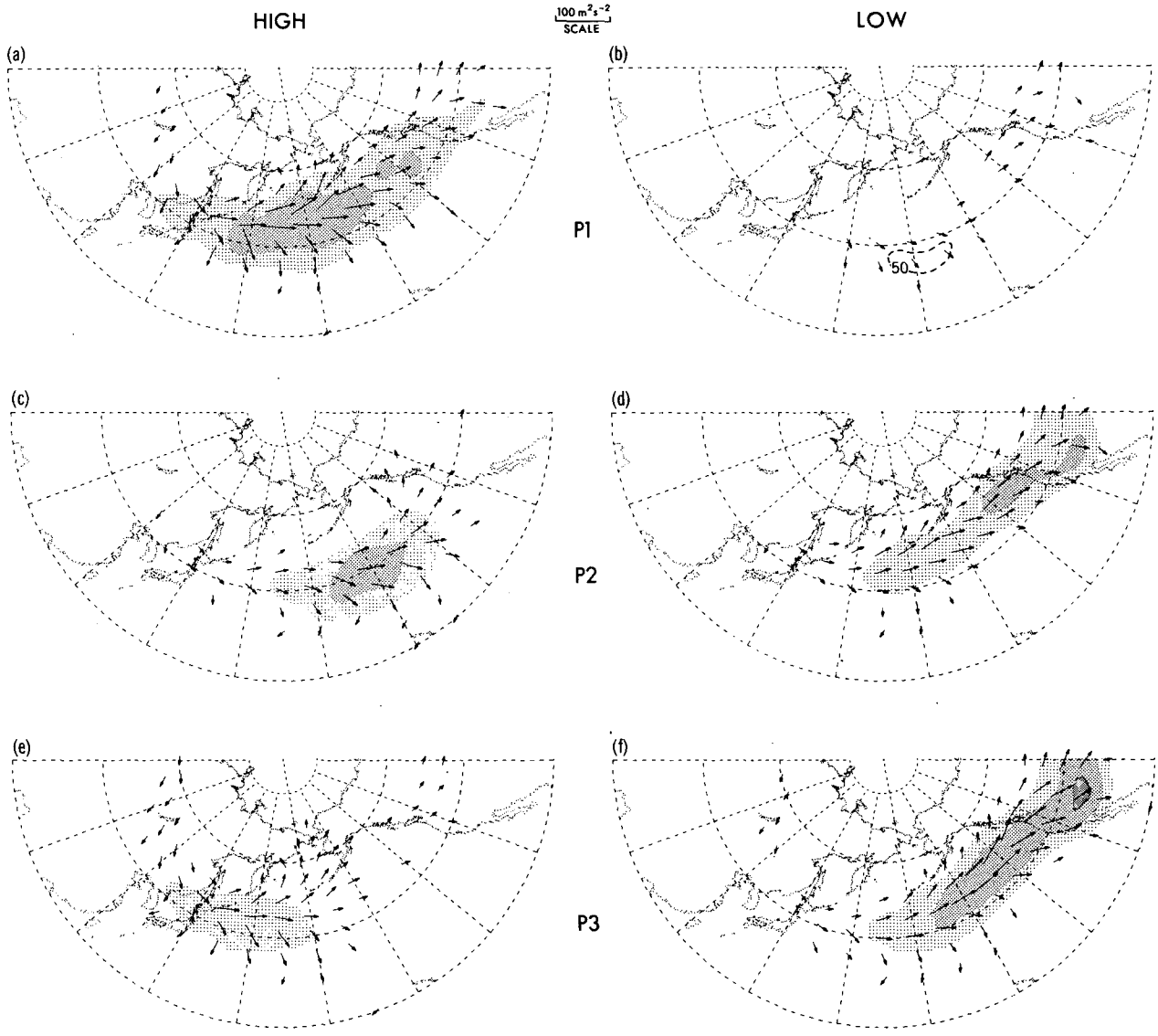

FIG. 9. High composite (left panels) and low composite (right panels) patterns of extended Eliassen–Palm vectors (arrows) and eddy kinetic energy (stippling) at 300 mb for the Pacific storm track eigenvectors P1, P2 and P3. Both quantities are based on geostrophic wind values derived from bandpass filtered geopotential height data. The scale for the arrow lengths is given at the top center of the figure. Eddy kinetic energy values falling within the ranges of 70–90, 90–110 and >110 $m^2 s^{-2}$ are indicated by light, medium and dense stippling, respectively. The dashed contour in panel (b) correspond to weak kinetic energy values of 50 $m^2 s^{-2}$.

that the time-filtered variance statistics for either the geopotential height or the wind fields are equally robust descriptors of the midlatitude storm tracks, and that the storm track eigenvectors documented in Figs. 2 and 3 are not too sensitive to the particular variable being analyzed. However, it is worth noting that whereas the pattern of $\overline{v'^2}$ is very similar to that of the rms of geopotential height for synoptic scale eddies (see Blackmon et al. 1977, Fig. 5b), the distribution for $\overline{u'^2}$ is characterized by a dumbbell shaped pattern, with highest amplitudes occurring just to the north and south of the maximum in $\overline{v'^2}$, so that the storm track axis corresponds to a saddle point (Blackmon et al. 1977, Fig. 5a). Taking also into account that $\overline{v'^2} > \overline{u'^2}$ for bandpass filtered data, one would expect the meridional width of the maximum in $\frac{1}{2}(\overline{u'^2} + \overline{v'^2})$ to be slightly larger than that of the corresponding feature in the rms of geopotential height.

Turning our attention now to the patterns of **E** in Figs. 9 and 10, and recalling the three applications of this diagnostic aid as outlined earlier, we note that the following features are common to most of the composite charts:

- Spatial variations of **E** along the storm tracks are generally weaker than variations transverse to the

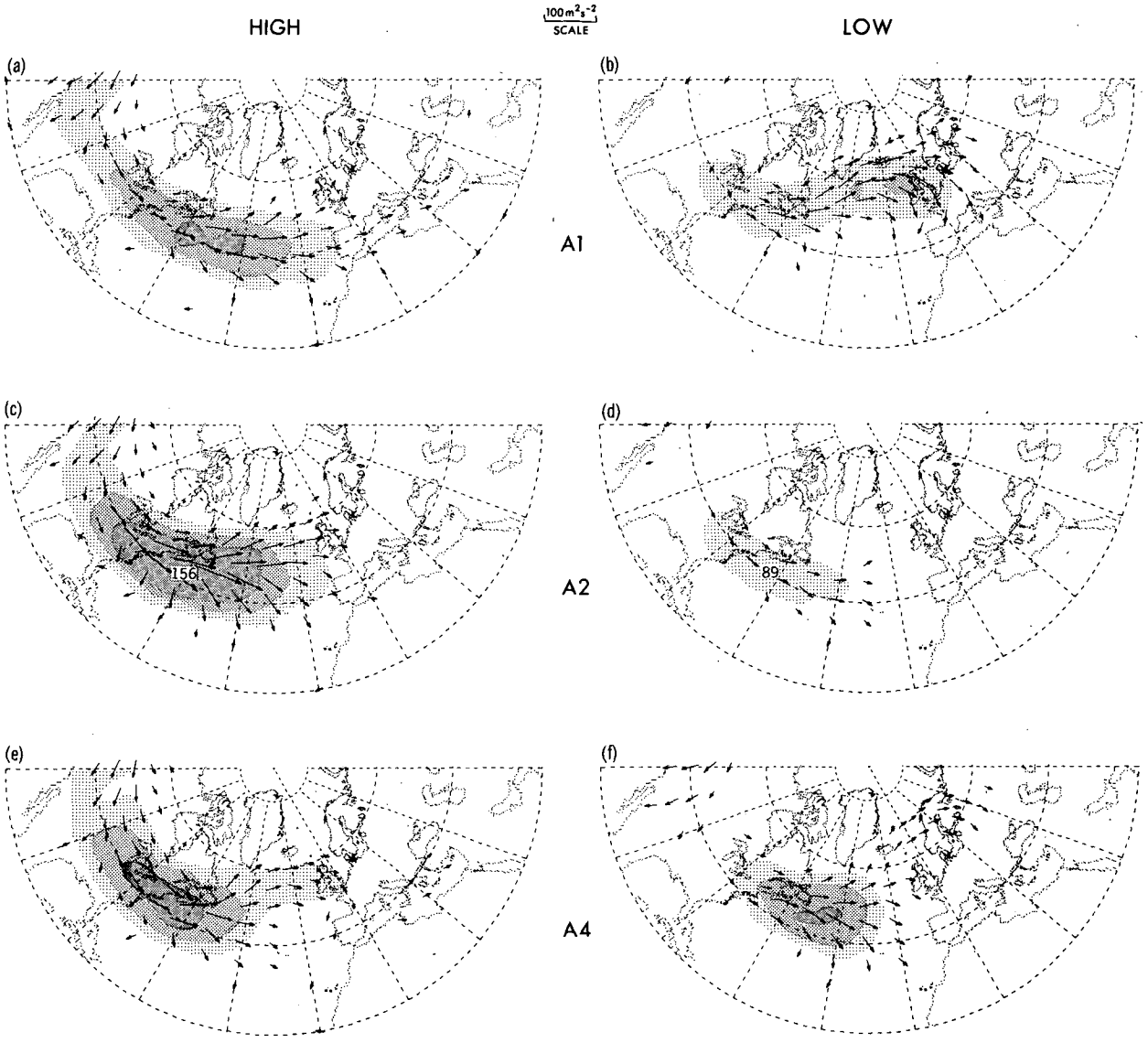

FIG. 10. As in Fig. 9, but for the Atlantic storm track eigenvectors A1, A2 and A4. Values of maximum kinetic energy are indicated in panels (c) and (d).

storm tracks, so that the divergence and curl of **E** are approximately given by derivatives in the meridional direction. For a given longitude, the meridional component of **E**, denoted as E_y, tends to diverge from the storm track axes, with poleward directed arrows north of the latitude of maximum kinetic energy, and equatorward arrows farther south. Hence the centers of eddy activity are characterized by $\partial E_y/\partial y = -\partial \overline{u'v'}/\partial y > 0$, and the eddy momentum transports, therefore, act to accelerate the westerly mean flow along the storm tracks. We also observe that, at a fixed meridian, the zonal component of **E**, denoted as E_x, is strongest near the storm track axes, and decreases in amplitude farther north and farther south, so that $-\partial E_x/\partial y = -\frac{1}{2}(\partial/\partial y)(\overline{v'^2} - \overline{u'^2})$ is positive poleward of the storm track axes, and negative in locations farther south. This configuration implies that the synoptic-scale eddies induce poleward accelerations of the mean flow north of the storm track axes, and equatorward accelerations in regions farther south. Some of the composite patterns shown here indicate a tendency for the **E** vectors to "fan out" at the eastern end of the storm tracks (e.g., Figs. 9c, 9e and 10f), with the arrows turning in a counterclockwise (clockwise) fashion north (south) of the downstream regions of the storm tracks. The derivative $\partial E_y/\partial x$ is therefore positive north of the exit zones of the storm tracks, and negative farther south. The corresponding mean flow acceleration is hence directed poleward (equatorward) in the sector situated northeast (southeast) of the center of eddy activity.

- The orientation of the minor axis of the eddy stress tensor may be estimated by taking half of the angle made by **E** with the longitudinal axis. Since **E** along the storm track axes is mostly dominated by the zonal component, the angles subtended with the zonal direction are small. In these locations, the minor and major axes are directed almost exactly east–west and north–south, respectively. This preferred elongation of the bandpass eddies along the meridional direction is consistent with the eastward directed **E** vectors, since $E_x = (\overline{v'^2} - \overline{u'^2})/2 > 0$ is a direct consequence of $\overline{v'^2} > \overline{u'^2}$. Immediately to the north of the storm track axes, the **E** vectors acquire a northeastward orientation, which implies that the major axis of the stress tensor (or, in synoptic terms, the trough and ridge axes) in these locations is tilted in the northwest–southeast direction. Analogously, the southeastward **E** vectors south of the storm track axes indicate the prevalence of southwest to northeast tilts of the eddy axes. The notable meridional changes in the orientation of the trough and ridge axes suggest that the disturbances are typically crescent shaped. Blackmon et al. (1984a,b) and Lau and Nath (1987) have arrived at similar conclusions on the basis of one-point teleconnection maps, and cross-spectral analysis, respectively. A closer scrutiny of some of the patterns for **E** reveals distinct changes in the shape of transient waves as they advance along certain storm tracks. The most striking example is given in the low composite for the A1 mode (Fig. 10b), which shows a storm track first curving northeastward upstream of the monthly mean ridge centered near 30°W (see contour field in Fig. 7b), and then southeastward downstream of the same ridge. The corresponding **E** vectors are mostly directed eastward upstream and north of the quasi-stationary pressure ridge, whereas their orientation over western Europe is seen to turn markedly towards the equator. This pattern indicates that the meridionally elongated fluctuations west of the ridge tend to evolve into zonally elongated disturbances farther downstream. This transformation in the eddy structure is also evident in the Atlantic blocking episode cited by Hoskins et al. (1983, Fig. 16), and in the composite of 17 blocking cases over the same region as constructed by Mullen (1987, Fig. 17a).
- The general direction of the eddy group velocity relative to the time mean flow, as inferred from the orientation of **E**, tends to be aligned with the axes of the corresponding storm tracks. The meridional component of **E** exhibits a distinct tendency to diverge from the storm track axes, thus indicating the occurrence of poleward and equatorward energy radiation from the centers of eddy activity. Comparison between the composite **E** fields and the accompanying monthly mean height contours (Figs. 6 and 7) offers a vivid illustration of the steering action of eddy energy propagation by the quasi-stationary flow pattern. It is seen that the **E** arrows follow closely the cyclonic and anticyclonic meanders of the local mean circulation. Particularly convincing examples of this eddy-mean flow relationship may be found in the high composite of P3 (Figs. 6e and 9e), the low composite of A1 (Figs. 7b and 10b), as well as the high and low composites of A4 (Figs. 7e, 7f and 10e, 10f).

b. Geopotential height tendencies

Although the **E** field yields considerable insights on eddy-induced accelerations of the mean flow, the inferences drawn from visual inspection of these patterns remain rather qualitative. Additional analysis tools are needed to present the intensity and vectorial nature of the eddy-forced circulation in a more explicit manner. A diagnostic technique which has proven to be useful for delineating the quantitative aspects of local eddy-mean flow interactions is the geopotential tendency method outlined in Lau and Holopainen (1984). This method makes use of the quasi-geostrophic potential vorticity equation to relate the temporal tendency of geopotential height to convergences of transient eddy fluxes of heat and vorticity. By examining climatological eddy statistics for an eight-winter period, Lau and Holopainen showed that the geopotential tendency in the upper troposphere is mostly determined by eddy vorticity fluxes. These authors further reported that the vertical variation of the geopotential height tendency associated with vorticity fluxes is characterized by an equivalent barotropic structure, with strongest amplitudes in the upper troposphere, and that the secondary circulations induced by the vorticity fluxes are generally rather weak. In view of the above findings, we shall restrict our present investigation to the geopotential tendency associated with vorticity fluxes at 300 mb. The three-dimensional formulation of Lau and Holopainen (1984) may then be simplified to a two-dimensional vorticity equation applicable at the 300 mb level, with the geopotential height tendency $\partial z/\partial t$ being expressed in terms of the inverse Laplacian of an eddy forcing term, i.e.,

$$\frac{\partial z}{\partial t} = \frac{f}{g} \nabla^{-2} \pi, \tag{1}$$

where

$$\pi \equiv \frac{1}{a^2 \cos\theta} \left(\frac{\partial}{\partial \theta} \frac{1}{\cos\theta} \frac{\partial}{\partial \theta} \cos^2\theta - \frac{1}{\cos\theta} \frac{\partial^2}{\partial \lambda^2} \right) \overline{u'v'} + \frac{1}{a^2 \cos^2\theta} \frac{\partial^2}{\partial \lambda \partial \theta} \cos\theta (\overline{u'^2} - \overline{v'^2}) \tag{2}$$

is the convergence of the transient eddy vorticity fluxes (see Holopainen, 1978, Eq. 14). Here a is the earth radius, f the Coriolis parameter, g the acceleration due to gravity, and λ, θ denote longitude and latitude, respectively.

Composite charts for $\partial z/\partial t$ were constructed using the same procedure described in sections 3c and 4a (see also footnote 2). For each winter month in a composite, the wind statistics u'^2, v'^2 and $\overline{u'v'}$ were computed using the bandpass filtered time series of 300 mb geostrophic wind data for that month. These statistics were substituted into Eq. 2 to obtain the forcing term π, and the associated geopotential tendency was then calculated by inverting the two-dimensional Laplacian in Eq. 1. The latter operation was accomplished using the subroutine PWSSSP in the NCAR software library. In order to lessen the impact on the solution due to the uncertain boundary condition at 20°N latitude, which corresponds to the southernmost extent of the NMC data, the solution to Eq. 1 was sought for the entire Northern Hemispheric domain, with the eddy forcing within the zone between 0° to 20°N being obtained by linear extrapolation from the known values at 20°N to uniformly zero values at the equator. Equation 1 was then solved by assuming that $\partial z/\partial t = 0$ at the equatorial boundary. In view of the somewhat arbitrary treatment of the buffer region between 0° and 20°N, we shall simply discard the solution for $\partial z/\partial t$ within that zone. A variety of numerical experiments suggest that the solution for $\partial z/\partial t$ poleward of 20°N is not sensitive to the particular procedure for specifying the condition at the southern boundary. Finally, summation of the monthly $\partial z/\partial t$ fields over the individual 10-month groups for each storm track eigenvector was performed to yield composites.

The difference patterns obtained by subtracting the low composites from the corresponding high composites are mapped in the right panels of Figs. 11 and 12, for the storm track eigenvectors of the Pacific and Atlantic Basins, respectively. For comparison with the accompanying monthly mean circulation patterns, the difference charts between the high and low composites for the monthly mean 300 mb heights are displayed in the left panels. The composite patterns in the left panels of Figs. 11 and 12 are qualitatively similar to the corresponding correlation charts shown in Figs. 4 and 5. The composite maps tend to place a stronger emphasis on the anomaly centers located poleward of 40°N, where the level of variability is generally higher than that in the subtropics. The features within the 20°–40°N zone show up much more clearly in the normalized correlation statistics presented in Figs. 4 and 5 (e.g., compare Fig. 4a with Fig. 11a).

Comparison between the distributions of $\partial z/\partial t$ in Figs. 11 and 12 and the corresponding eigenvector patterns in Figs. 2 and 3 confirms many of the inferences on eddy-induced acceleration drawn earlier from the **E** vectors. For instance, zonally elongated positive extrema in the eigenvector patterns (i.e., above-normal synoptic-scale activity) are accompanied by positive height tendencies immediately to the south, negative height tendencies to the north, and eastward accelerations at the sites of the extrema. The northward (southward) accelerations occurring north (south) of the downstream region of these positive extrema are consistent with the cyclonic (anticyclonic) curvature of the **E** vectors in these regions. The reverse situation is seen to hold for zonally elongated negative extrema in the eigenvectors. In summary, we discern a near-quadrature spatial relationship between the distribution of $\partial z/\partial t$ and the corresponding eigenvector patterns. Monopolar eigenvector modes of the rms height statistics (i.e., P1, A2) are characterized by geopotential tendencies with a dipolar configuration (Figs. 11b and 12d). Dipolar eigenvector modes (i.e., P2, A1) are concurrent with height tendency patterns having three principal extrema (Figs. 11d and 12b), so that nodes in the eigenvector coincide with antinodes in the height tendency field, and vice versa.

It was observed in section 3b that the storm track eigenvectors are closely related to the monthly mean circulation. The monopolar eigenvector modes were shown to be associated with the dipolar WP and WA teleconnection patterns, whereas the dipolar modes are correlated with the more wave-like PNA and EA patterns. Hence, the storm tracks are not only in near-quadrature with the geopotential tendency patterns, but they also exhibit an analogous phase relationship with the monthly averaged height anomalies. These results imply that the monthly mean height anomalies and the eddy-forced height tendencies should also bear well-defined spatial relationships with each other. Comparison between the left and right panels in Figs. 11 and 12 reveals that the height composite for a given mode indeed resembles the eddy-induced height tendency composite for the same mode. This correspondence is particularly evident for the Atlantic modes (Fig. 12), in which each anomaly center in the 300 mb height composite may be identified with an extremum of the same polarity in the composite for $\partial z/\partial t$. The spatial correlation between the height and geopotential tendency composites is somewhat weaker for the Pacific modes (Fig. 11).

The spatial resemblance between the left and right panels in Figs. 11 and 12 is suggestive of a near in-phase relationship between the barotropic eddy forcing and the prevalent monthly mean circulation. The characteristic time scale of this forcing, as estimated by taking the ratio of the amplitudes of the monthly mean height anomalies to those of the geopotential tendencies at representative sites, is approximately 7–10 days.

In order to ascertain the generality of the spatial relationship between eddy forcing and the monthly mean flow, as well as to identify those geographical regions where this relationship is most prominent, we have constructed the $\partial z/\partial t$ field at 300 mb for every winter month in the 90-month dataset, and then computed the temporal correlation coefficient between the values of $\partial z/\partial t$ at each grid point and the values of monthly mean 300 mb height at the same grid point. Clima-

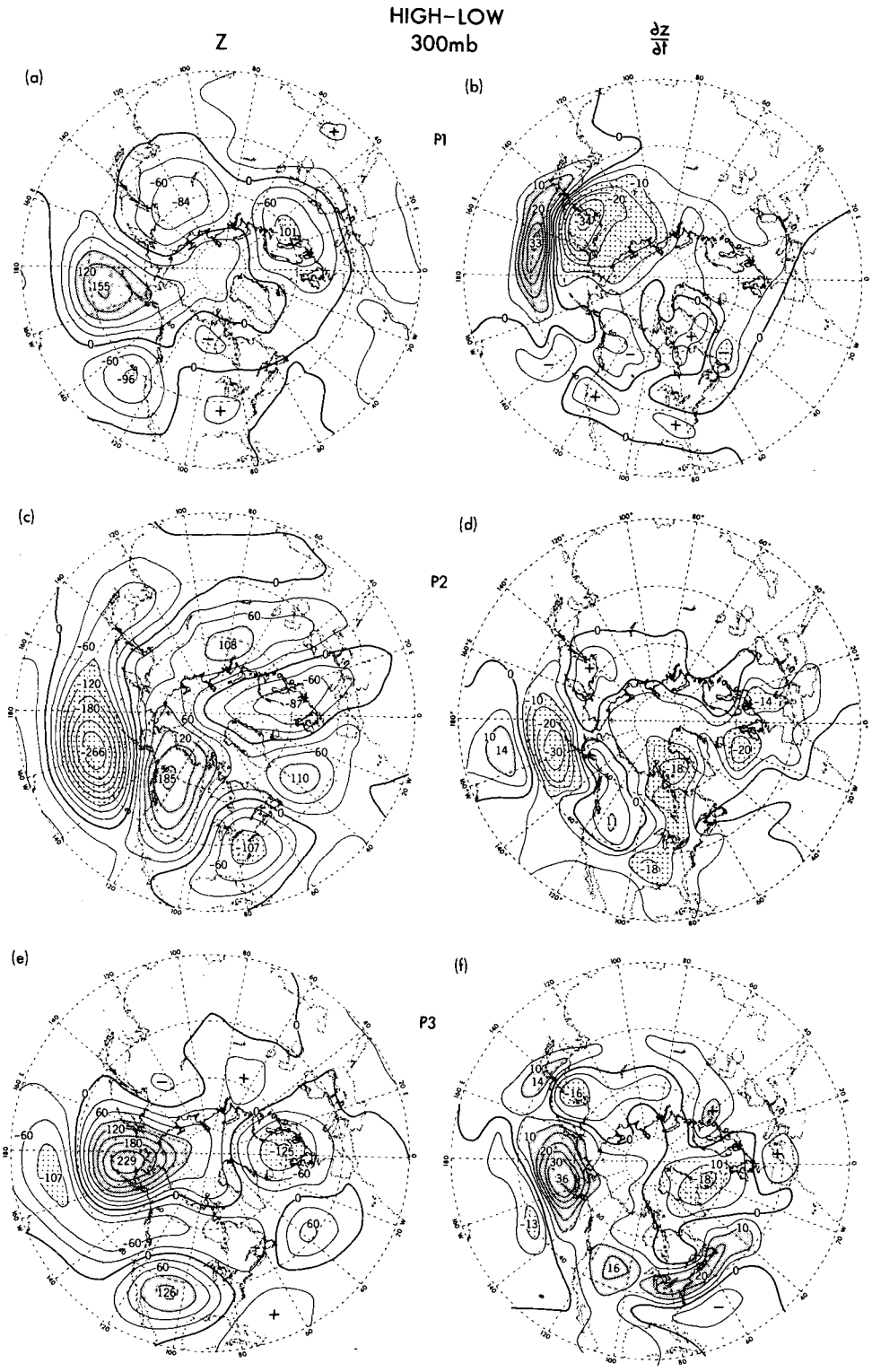

FIG. 11. Difference charts obtained by subtracting the low composites from the corresponding high composites of monthly averaged 300 mb height (left panels, contour interval is 30 m) and 300 mb height tendency associated with vorticity transports by bandpass eddies (right panels, contour interval is 5×10^{-5} m s^{-1}), for Pacific storm track eigenvectors P1, P2 and P3. Regions with large positive and negative values are depicted by dense and light stippling, respectively.

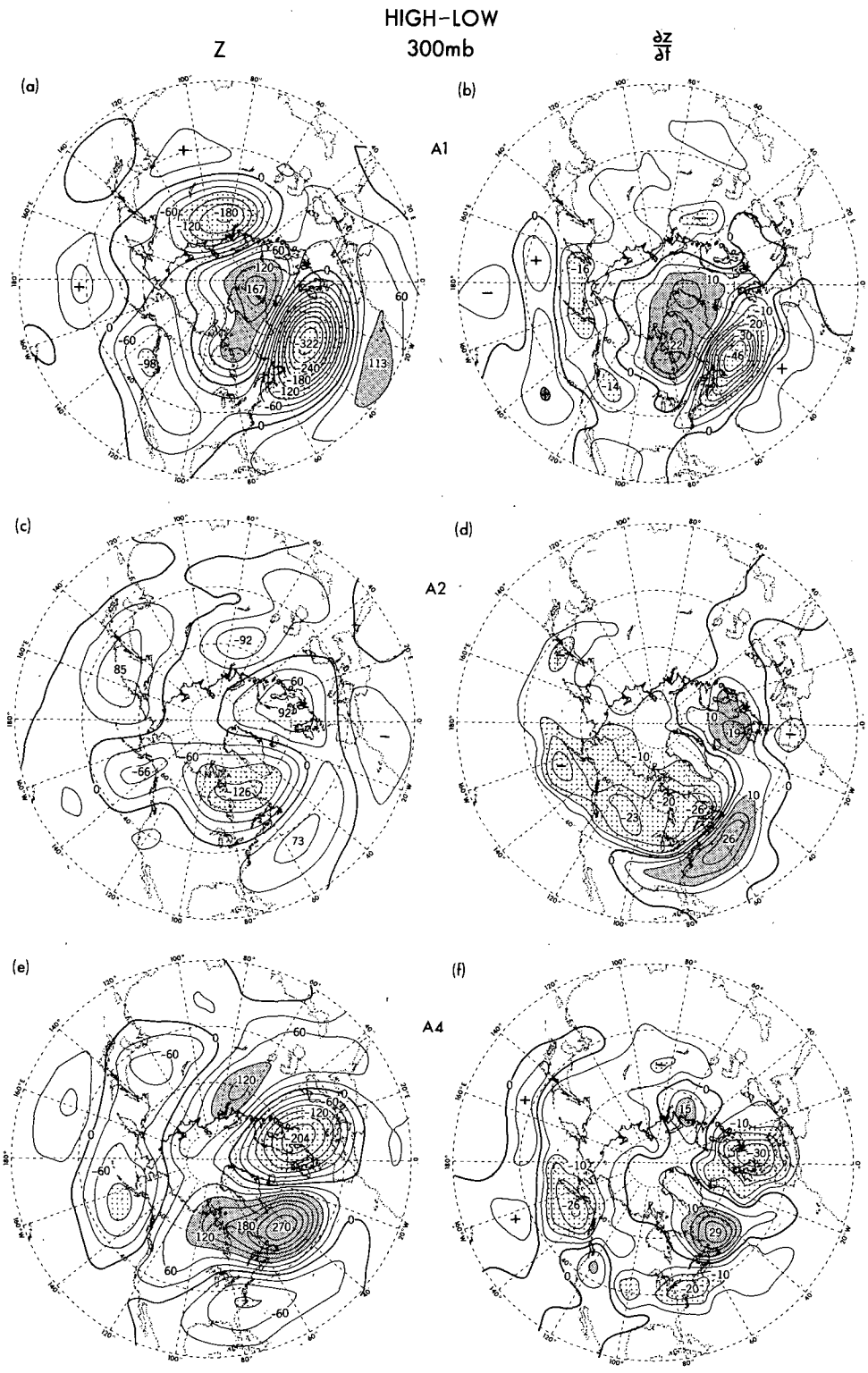

FIG. 12. As in Fig. 11, but for Atlantic eigenvectors A1, A2 and A4.

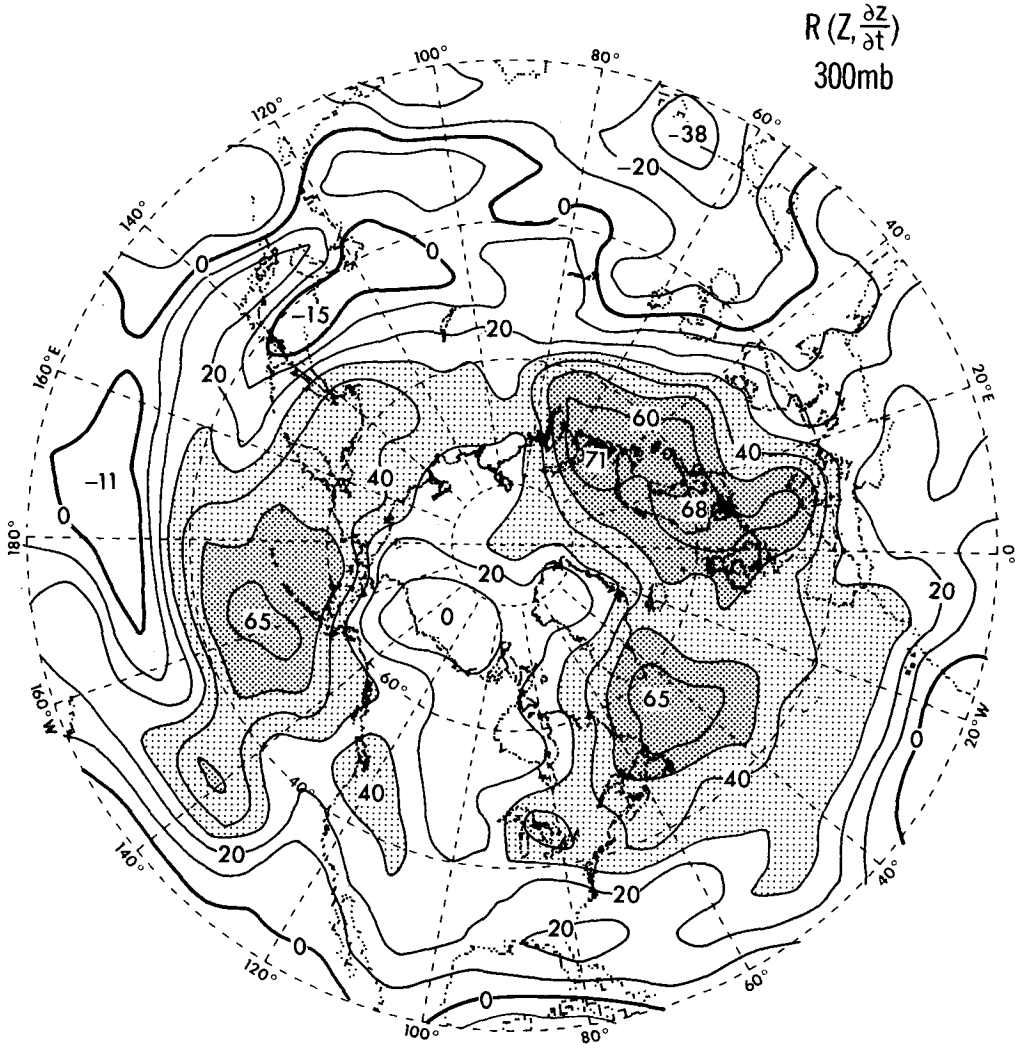

FIG. 13. Distribution of temporal correlation coefficients (in percent) between monthly averaged 300 mb height and the local 300 mb height tendency associated with vorticity transports by bandpass eddies. Contour interval is 10%. Regions with correlation values exceeding 30% and 50% are depicted by light and dense stippling, respectively.

tological seasonal cycles for $\partial z/\partial t$ and monthly mean height have been removed in these calculations. In Fig. 13 the hemispheric distribution of the correlation coefficients thus obtained is shown. It is seen that the correlation is positive throughout much of the extratropics, with centers of maximum occurring near the Aleutians, Labrador Sea and northern Europe. These areas of strong positive correlations are coincident with enhanced geopotential height fluctuations with time scales between 10 days and a season, as can be inferred from the maxima appearing in the rms pattern for lowpass filtered data shown in Lau and Nath (1987, Fig. 1c). These same regions are also noted for the frequent occurrence of persistent, high-amplitude meteorological anomalies (Dole 1983, Fig. 4.2).

Mullen (1987) has also investigated the nature of synoptic-scale eddy forcing during representative North Atlantic blocking events. He noted that the positive geopotential tendency associated with eddy vorticity fluxes is centered approximately 20° longitude upstream of the blocking ridge at 300 mb (see his Fig. 5c). The results presented by Holopainen and Fortelius (1987, Figs. 2a and 4a) for a single blocking episode in February 1979 also suggest that the maximum eddy forcing is located slightly west of the pressure ridge over western Europe. A careful inspection of the composite patterns for the A1 mode (Figs. 12a and 12b), which is known to be related to North Atlantic blocking, reveals that the extremum of eddy-induced geopotential tendency near 50°N, 45°W is shifted westward by about 10° longitude relative to the corresponding extremum in the composite monthly mean height field. However, there also exist in Figs. 11 and 12 many other situations when extrema in the right

and left panels occur over almost the same sites. The strong positive correlation coefficients in Fig. 13 over northern Europe as well as the extratropical North Pacific and North Atlantic suggest that, in a statistical sense, collocation of the eddy forcing and height anomaly tends to prevail in the 90-month sample examined here.

In presenting the difference maps in Figs. 11 and 12, we have implicitly assumed that the relationships between the eddy-induced tendency and the monthly mean circulation hold equally well for the positive and negative phases of each eigenvector mode. The validity of this assumption may be evaluated by comparing the high composite anomaly patterns of $\partial z/\partial t$ and monthly averaged heights for a given storm track mode with the corresponding low composite patterns. An example of such a comparison is given in Fig. 14, which shows separately the high and low composites for the A1 mode. It is seen that the strong spatial relationships between the eddy forcing and the monthly mean circulation are evident in both the positive and negative phases of A1. In particular, the slight westward displacement of the extremum in $\partial z/\partial t$ near 50°N, 45°W relative to the monthly mean height anomaly, as noted in the preceding paragraph, is discernible when the anomalous circulation over the North Atlantic is either cyclonic (see Figs. 14a and 14b) or anticyclonic (Figs. 14c and 14d). Inspection of the high and low composites for the other eigenvector modes (not shown) also indicates that, except for a sign reversal, the opposite phases of each mode are characterized by rather similar anomaly patterns of $\partial z/\partial t$ and monthly mean heights. We hence conclude that the spatial relationships between transient eddy forcing and the quasi-stationary circulation do not exhibit any notable dependence on the polarity of the circulation anomalies.

5. Circulation changes at sea level associated with storm track variability

In order to describe the characteristic circulation patterns at sea level related to different modes of variability in the midtropospheric storm tracks, the procedure outlined in section 3c has been used to compute high and low composites of the monthly averaged sea level pressure (SLP) field from the NMC dataset. These SLP composites are hence averages for the 10-month groups listed in Table 2, which have been determined on the basis of the coefficients for the storm track eigenvectors at the 500 mb level. The difference charts obtained by subtracting the low composites of the SLP field from the corresponding high composites are displayed in Figs. 15 and 16 for the Pacific and Atlantic eigenvectors, respectively.

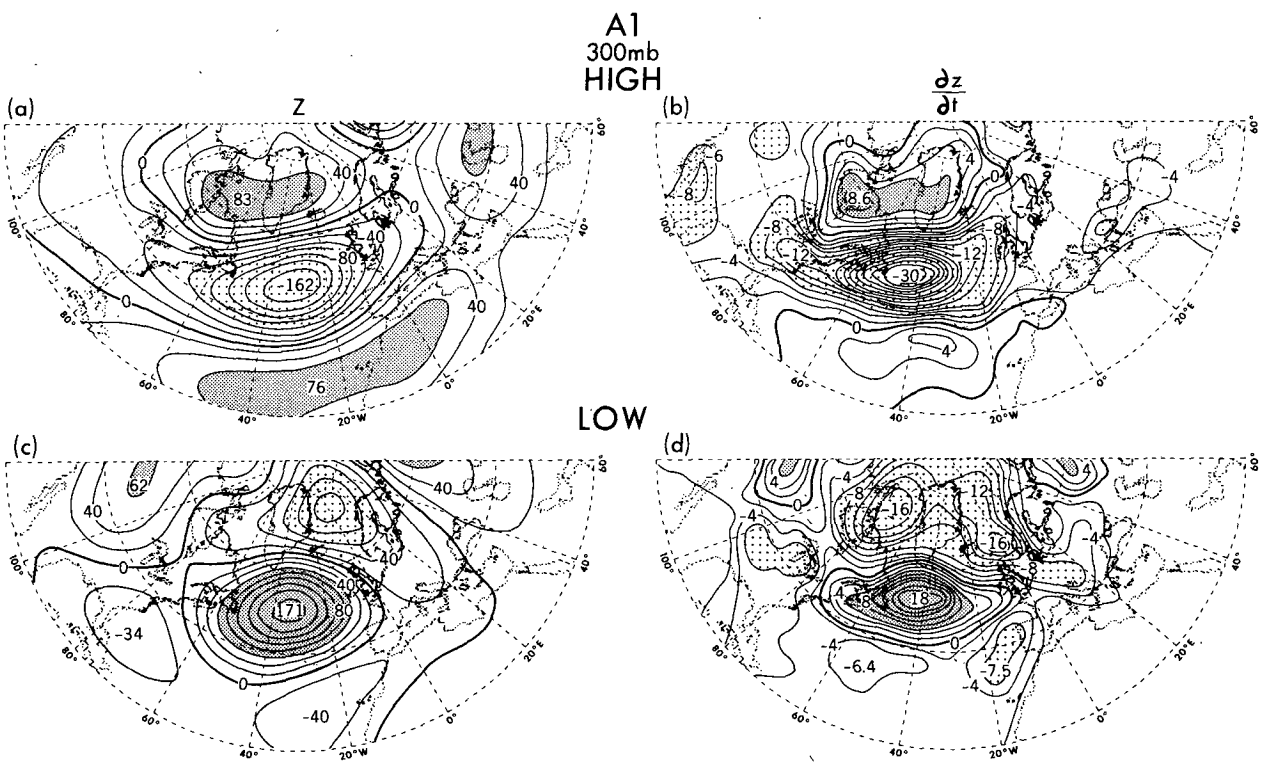

FIG. 14. High composite (upper panels) and low composite (lower panels) anomaly patterns of 300 mb height (left, contour interval is 20 m) and 300 mb height tendency associated with vorticity transports by bandpass eddies (right, contour interval is 2×10^{-5} m s^{-1}), for Atlantic storm track eigenvector A1. Regions with large positive and negative values are depicted by dense and light stippling, respectively.

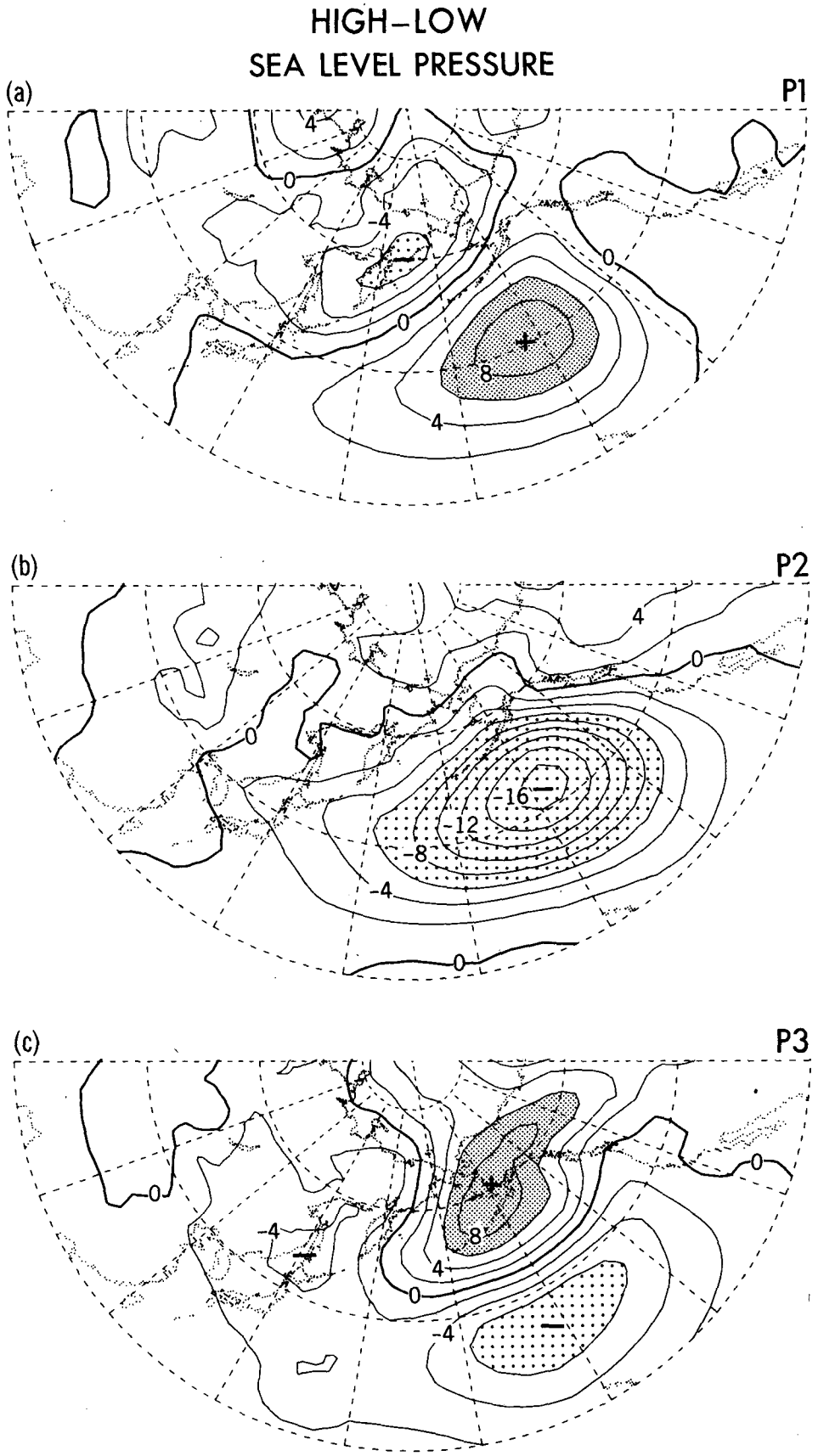

FIG. 15. Difference charts obtained by subtracting the low composites from the corresponding high composites of monthly averaged sea level pressure, for Pacific storm track eigenvectors P1, P2 and P3. Contour interval is 2 mb. Regions with values above +6 mb and below −6 mb are depicted by dark and light stippling, respectively.

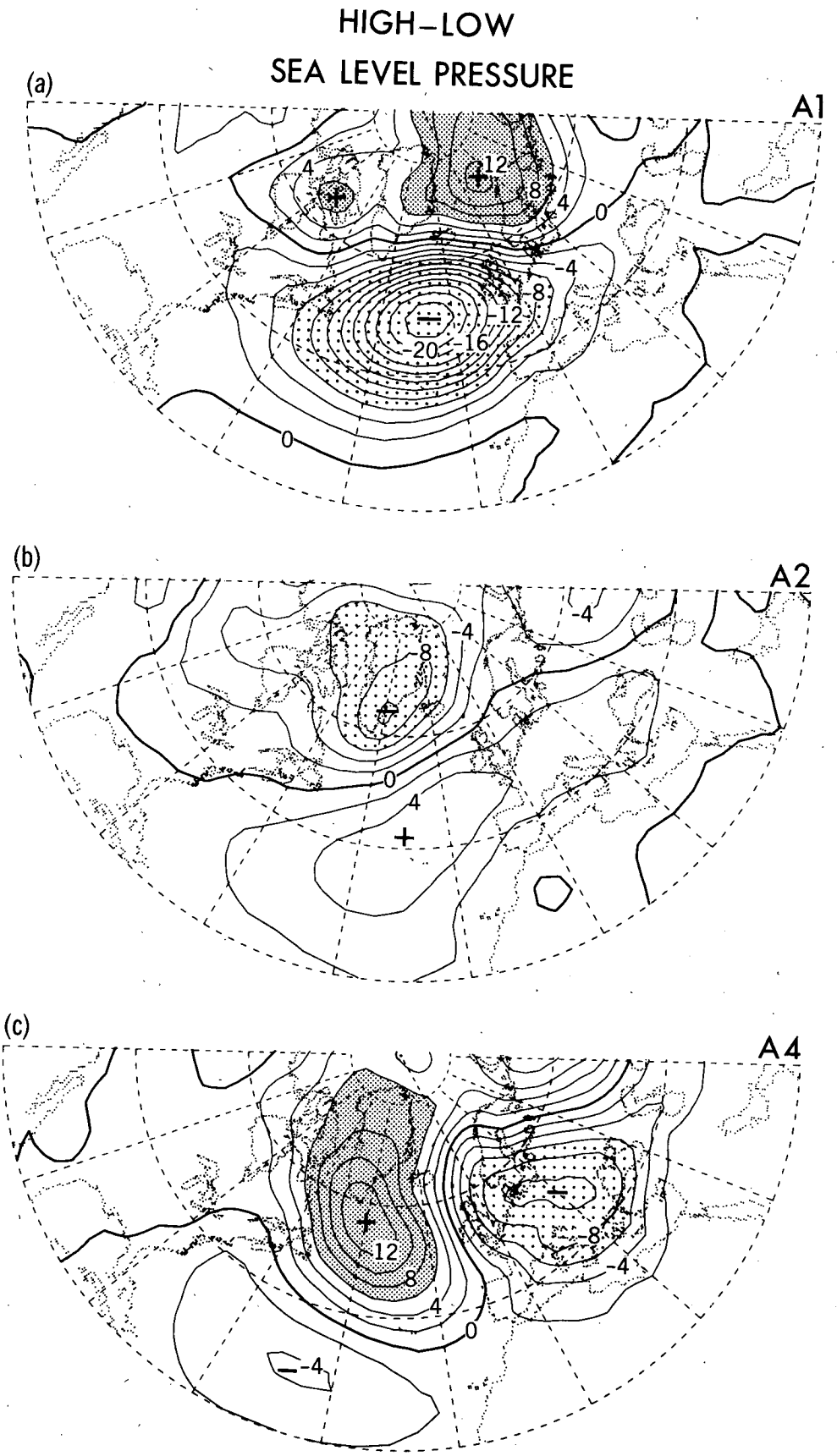

FIG. 16. As in Fig. 15, but for Atlantic storm track eigenvectors A1, A2 and A4.

Comparison between the 300 mb height composite for the Pacific modes, shown in the left panels of Fig. 11, and the SLP composites in Fig. 15 indicates considerable spatial resemblance between the monthly mean anomalies at the two levels, especially over the maritime areas. This result is consistent with the strong local correlations between monthly averaged heights at various tropospheric layers over the two ocean basins, as was pointed out by Blackmon et al. (1979, Fig. 2). For the P1 mode, the extremum over the Kamchatka Peninsula in the SLP pattern (Fig. 15a) is displaced eastward of the corresponding feature at 300 mb (Fig. 11a) by almost 40° of longitude. Another noteworthy phenomenon in the SLP field is the tendency for the Aleutian anomaly in the P3 pattern (Fig. 15c) to spread across the Alaskan Peninsula towards the leeslopes of the Canadian Rockies. The polarity of the near-surface fluctuations in the latter region is hence opposite to that at 300 mb (Fig. 11e). This baroclinic behavior on the leeward side of the Rocky Mountains has been noted in the Pacific (P) pattern described by Hsu and Wallace (1985, left panel of Fig. 5). The overall pattern in Fig. 15c also resembles that associated with the North Pacific Oscillation (Rogers 1981, Fig. 3).

The maritime features in the SLP patterns for the Atlantic modes (Fig. 16) also exhibit a strong correspondence with their counterparts in the upper troposphere (left panels of Fig. 12). The Greenland SLP anomaly in the A2 mode (Fig. 16b) is seen to be located considerably east of the 300 mb center over the Labrador Peninsula–Hudson Bay region (Fig. 12c). The surface circulation associated with the A2 mode is also reminiscent of the characteristic pattern accompanying the wintertime temperature seesaw between Greenland and northern Europe, as documented by van Loon and Rogers (1978, Fig. 3).

The eigenvector patterns for the midtropospheric storm tracks (Figs. 2 and 3) are evidently related to the monthly mean circulation at sea level. Above normal eddy activity at 500 mb is seen to be associated with enhanced surface westerlies equatorward of negative SLP anomalies, whereas the eddy amplitudes are reduced in regions with anomalous surface easterlies.

6. Discussion

This study has been devoted to a better understanding of the relationships and interactions between two distinct classes of atmospheric fluctuations with disparate time scales. The first type of disturbances correspond to weather systems with typical periods of several days. The second type consists of those slowly varying phenomena which retain their identities on monthly mean charts. We have identified a set of well-defined relationships between the behavior of the synoptic-scale eddies and the spatial configuration of the monthly averaged circulation anomalies. As is evident from the composite charts in Figs. 6 and 7, the correspondence between the storm tracks and the concurrent monthly mean flow pattern is so robust that one could locate with little difficulty the regions of enhanced eddy activity by inspection of monthly averaged 500 mb height charts alone. The strong association between the storm tracks and the low-frequency component of the circulation allows for a systematic investigation of the dynamical forcing of the quasi-stationary flow by the synoptic-scale eddies. It is shown that the barotropic eddy forcing is nearly in phase with the monthly mean anomalies.

We began our analysis of the eddy-mean flow problem by partitioning the first- and second-moment statistics according to the conventional monthly calendar, and then by exploring relationships among various quantities for individual months. Whereas the monthly calendar offers a convenient framework for organizing the dataset, the approach adopted here may not be the optimal procedure for capturing the outstanding synoptic events of interest. For instance, a strong signal which happens to fall within the latter part of a certain month and the first part of the following month would be poorly represented in the time-average for either month. An alternative approach is to identify the precise dates for the occurrence of individual episodes by a set of predetermined criteria, and to examine the data for these interesting time periods exclusively. The advantages of this methodology have been exploited in the case studies by Dole and Gordon (1983), Illari (1984), Mullen (1987) and Holopainen and Fortelius (1987). In comparing the findings from the latter studies with those based on continuous time series such as the present work, one needs to recognize that the case-study approach is focused on atmospheric phenomena which meet rather specific standards, whereas correlation analyses of entire datasets are aimed at atmospheric behavior common to a wide diversity of circulation types. A case in point is the maintenance of the unique flow configuration and persistence characteristics associated with the blocking ridges. By examining 17 blocking events occurring over 20 winters, Mullen (1987) presented convincing evidence of the preference of the anticyclonic eddy forcing to be located distinctly upstream of quasi-stationary high pressure ridges. On the other hand, the correlation chart in Fig. 13 of this study, which is constructed on the basis of all 90 winter months available in our data archive, suggests that the eddy forcing generally exhibits considerably less spatial displacement from the corresponding monthly mean circulation anomaly. Hence the behavior of high-frequency transients during blocking episodes appears to be rather exceptional.

In the present study, we have emphasized the forcing by eddy vorticity fluxes of the upper tropospheric flow. Bearing in mind the highly baroclinic nature of the cyclone eddies, the heat fluxes associated with the bandpass fluctuations cannot be ignored in any com-

plete treatment of the eddy-mean flow interaction problem. The geopotential tendency calculations performed by Lau and Holopainen (1984, Figs. 3 and 4) indicate that the forcing at the 300 mb level due to eddy heat transports is opposite to, but considerably weaker than the forcing due to eddy vorticity transports. Hence, the inclusion of the effects of eddy heat fluxes would not alter the qualitative aspects of the inferences drawn from the barotropic calculations in section 4b. However, Lau and Holopainen noted that the eddy forcing at 1000 mb is dominated by the eddy heat fluxes, with the tendency associated with the baroclinic effects being almost in phase with that due to barotropic processes. A full description of the eddy effects associated with various storm track configurations must await the solution of the three-dimensional geopotential tendency equation forced by composites of both heat and vorticity fluxes for all pressure levels in the atmospheric column.

In computing the eddy vorticity fluxes, the variance and covariance circulation statistics were compiled using geostrophic wind data. Effects associated with the divergent component of the transient motion are hence neglected in our calculations. Hoskins and Sardeshmukh (1987) have recently pointed out that the convergence of vorticity transport due to the divergent eddy flow field is comparable to its counterpart associated with the rotational component. The results in section 4 of our study should therefore be interpreted with this approximation in mind.

We have thus far been concerned with the simultaneous relationships between the storm tracks and various characteristic teleconnection patterns on a month-to-month basis. It is equally important to determine if systematic temporal leads or lags exist between the occurrence of the synoptic-scale eddies and the establishment of the slowly varying teleconnection patterns. Our synoptic experience suggests that such temporal lags would be rather short, perhaps on the order of several days. These lag relationships could also exhibit a considerable geographical dependence, so that their precise nature may vary for different teleconnection patterns. To address these issues properly, the temporal evolution of high- and low-frequency components of the circulation needs to be examined on time scales much shorter than the monthly intervals used here. A fuller understanding of such temporal behavior would yield fresh insights on the fundamental role of baroclinic waves in the atmospheric general circulation; i.e., Is the occurrence of these transient disturbances simply a passive response to the planetary wave pattern, or do these disturbances actively contribute to the establishment of persistent circulation anomalies?

The subweekly time scale has been chosen for the present analysis primarily because it is associated with baroclinic instability. Blackmon et al. (1984a,b) have discerned several other frequency bands in the atmospheric spectrum which are of equal interest. In particular, these authors have interpreted circulation features with intermediate time scales between 10 and 30 days in terms of Rossby wave dispersion, whereas those phenomena with even longer periods have been identified with barotropically unstable fluctuations (see Simmons et al. 1983). Furthermore, Wallace and Lau (1985) have pointed out that the patterns of extended Eliassen–Palm fluxes for these longer time scales are radically different from those associated with synoptic-scale eddies. Lau and Holopainen (1984) have also shown that the eddy-induced geopotential tendency in the upper troposphere is largely determined by vorticity transports by disturbances with characteristic periods of 10 days and longer, and that the forcing associated with these low-frequency eddies exhibits a near out-of-phase relationship with the stationary wave. In view of the rather distinct behavior of perturbations with longer time scales, it would be of considerable interest to apply the analysis tools developed here to these low-frequency phenomena. Our understanding of the nature of atmospheric variability would not be complete without a comprehensive investigation of the myriad interactive processes involving the multiple frequency ranges noted above.

Acknowledgments. I am indebted to Isaac M. Held and John M. Wallace for stimulating discussions on various aspects of this study, and to Mary Jo Nath for assembling the necessary datasets for this investigation. I would also like to thank Abraham H. Oort and Masahide Kimoto for examining the manuscript and offering helpful comments. The constructive reviews by the two official referees have led to useful clarifications of some of the findings in this study. The figures were drafted by the Scientific Illustration Group at GFDL. Preparation of the manuscript was assisted by Joyce Kennedy and Wendy Marshall.

REFERENCES

Barnston, A. G., and R. E. Livezey, 1987: Classification, seasonality and persistence of low-frequency atmospheric circulation patterns. *Mon. Wea. Rev.*, **115**, 1083–1126.

Blackmon, M. L., 1976: A climatological spectral study of the 500 mb geopotential height of the Northern Hemisphere. *J. Atmos. Sci.*, **33**, 1607–1623.

——, J. M. Wallace, N.-C. Lau and S. L. Mullen, 1977: An observational study of the Northern Hemisphere wintertime circulation. *J. Atmos. Sci.*, **34**, 1040–1053.

——, R. A. Madden, J. M. Wallace and D. S. Gutzler, 1979: Geographical variations in the vertical structure of geopotential height fluctuations. *J. Atmos. Sci.*, **36**, 2450–2466.

——, Y.-H. Lee and J. M. Wallace, 1984a: Horizontal structure of 500 mb height fluctuations with long, intermediate and short time scales. *J. Atmos. Sci.*, **41**, 961–979.

——, ——, —— and H.-H. Hsu, 1984b: Time variation of 500 mb height fluctuations with long, intermediate and short time scales as deduced from lag-correlation statistics. *J. Atmos. Sci.*, **41**, 981–991.

Dole, R. M., 1983: Persistent anomalies of the extratropical Northern Hemisphere wintertime circulation. In *Large Scale Dynamical*

Processes in the Atmosphere, B. J. Hoskins and R. P. Pearce, Eds., Academic Press, 95–109.

——, 1986: Persistent anomalies of the extratropical Northern Hemisphere wintertime circulation: Structure. *Mon. Wea. Rev.*, **114,** 178–207.

——, and N. D. Gordon, 1983: Persistent anomalies of the extratropical Northern Hemisphere wintertime circulation: Geographical distribution and regional persistence characteristics. *Mon. Wea. Rev.*, **111,** 1567–1586.

Esbensen, S. K., 1984: A comparison of intermonthly and interannual teleconnection in the 700 mb geopotential height field during the Northern Hemisphere winter. *Mon. Wea. Rev.*, **112,** 2016–2032.

Frederiksen, J. S., 1979: The effects of long planetary waves on the regions of cyclogenesis: Linear theory. *J. Atmos. Sci.*, **36,** 195–204.

Green, J. S. A., 1977: The weather during July 1976: Some dynamical considerations of the drought. *Weather,* **32,** 120–128.

Hendon, H. H., and D. L. Hartmann, 1985: Variability in a nonlinear model of the atmosphere with zonally symmetric forcing. *J. Atmos. Sci.*, **42,** 2783–2797.

Holopainen, E. O., 1978: On the dynamic forcing of the long-term mean flow by the large-scale Reynolds' stresses in the atmosphere. *J. Atmos. Sci.*, **35,** 1596–1604.

——, 1984: Statistical local effect of synoptic-scale transient eddies on the time-mean flow in the northern extratropics in winter. *J. Atmos. Sci.*, **41,** 2505–2515.

——, and C. Fortelius, 1987: High-frequency transient eddies and blocking. *J. Atmos. Sci.*, **44,** 1632–1645.

Hoskins, B. J., and P. D. Sardeshmukh, 1987: Transient eddies and the seasonal mean rotational flow. *J. Atmos. Sci.*, **44,** 328–338.

——, I. N. James and G. H. White, 1983: The shape, propagation and mean-flow interaction of large-scale weather systems. *J. Atmos. Sci.*, **40,** 1595–1612.

Hsu, H.-H., and J. M. Wallace, 1985: Vertical structure of wintertime teleconnection patterns. *J. Atmos. Sci.*, **42,** 1693–1710.

Illari, L., 1984: A diagnostic study of the potential vorticity in a warm blocking anticyclone. *J. Atmos. Sci.*, **41,** 3518–3526.

Kutzbach, J. E., 1967: Empirical eigenvectors of sea level pressure, surface temperature and precipitation complexes over North America. *J. Appl. Meteor.*, **6,** 791–802.

Lau, N.-C., 1978: On the three-dimensional structure of the observed transient eddy statistics of the Northern Hemisphere wintertime circulation. *J. Atmos. Sci.*, **35,** 1900–1923.

——, and E. O. Holopainen, 1984: Transient eddy forcing of the time-mean flow as identified by geopotential tendencies. *J. Atmos. Sci.*, **41,** 313–328.

——, and M. J. Nath, 1987: Frequency dependence of the structure and temporal development of wintertime tropospheric fluctuations—comparison of a GCM simulation with observations. *Mon. Wea. Rev.*, **115,** 251–271.

Mullen, S. L, 1987: Transient eddy forcing of blocking flows. *J. Atmos. Sci.*, **44,** 3–22.

Petterssen, S., 1956: *Weather Analysis and Forecasting, Vol. 1,* McGraw Hill, 267–276.

Plumb, R. A., 1985: On the three-dimensional propagation of stationary waves. *J. Atmos. Sci.*, **42,** 217–229.

——, 1986: Three-dimensional propagation of transient quasi-geostrophic eddies and its relationship with the eddy forcing of the time-mean flow. *J. Atmos. Sci.*, **43,** 1657–1670.

Rogers, J. C., 1981: The North Pacific Oscillation. *J. Climatol.*, **1,** 39–57.

Simmons, A. J., and B. J. Hoskins, 1978: The life cycles of some nonlinear baroclinic waves. *J. Atmos. Sci.*, **35,** 414–432.

——, J. M. Wallace and G. W. Branstator, 1983: Barotropic wave propagation and instability, and atmospheric teleconnection patterns. *J. Atmos. Sci.*, **40,** 1363–1392.

Trenberth, K. E., 1986: An assessment of the impact of transient eddies on the zonal flow during a blocking episode using localized Eliassen–Palm flux diagnostics. *J. Atmos. Sci.*, **43,** 2070–2087.

van Loon, H., and J. C. Rogers, 1978: The seesaw in winter temperatures between Greenland and Northern Europe. Part I: General description. *Mon. Wea. Rev.*, **106,** 296–310.

Wallace, J. M., and D. S. Gutzler, 1981: Teleconnections in the geopotential height field during the Northern Hemisphere winter. *Mon. Wea. Rev.*, **109,** 784–812.

——, and N.-C. Lau, 1985: On the role of barotropic energy conversion in the general circulation. *Adv. Geophys.*, **28A,** 33–74.

——, G-H. Lim and M. L. Blackmon, 1988: On the relationship between cyclone tracks, anticyclone tracks and baroclinic waveguides. *J. Atmos. Sci.*, **45,** 439–462.